Success probabilities in time-reversal-based hybrid quantum state transfer

Kevin Randles[*] and S. J. van Enk[†]

Department of Physics and Center for Optical, Molecular and Quantum Science, University of Oregon, Eugene, Oregon 97403, USA

(Received 23 December 2023; revised 15 May 2024; accepted 28 May 2024; published 3 July 2024)

We consider two memory nodes of a quantum network connected by flying qubits. We are particularly interested in the case where a flying qubit produced by one node has to be transformed before it can interface efficiently with the next node. Such transformations can be utilized as a key part of the distribution of quantum states and hence entanglement between the nodes of a hybrid quantum network linking together different quantum technologies. We show how and why the probability of interfacing successfully is determined by the overlap of the spectral shape of the actual flying qubit and the ideal shape. This allows us to analytically and numerically analyze how the probability of success is impacted by realistic errors, and show the utility of our scheme (in consonance with known error correction methods) in connecting hybrid nodes of a quantum network. We focus here on a concrete implementation in which the memory nodes consist of three-level atoms in cavities and the flying qubits are photons.

DOI: 10.1103/PhysRevA.110.012415

I. GENERAL INTRODUCTION

The quantum internet [1] is envisioned to allow the implementation of various quantum communication, computation, and measurement (sensing) tasks that improve upon their classical counterparts. Scaling the underlying networks to connect a larger numbers of quantum processor systems, often referred to as nodes in the context of quantum communication, improving these processors, and controlling their robustness against noise are among important current practical issues [2,3]. The fundamental building blocks of these networks are the nodes themselves and the quantum transmission lines (also called quantum channels) that serve as the network edges. Such an edge links together two nodes so that quantum information, say the state of a qubit, can be sent between them at will. These nodes may range from simple devices operating on small numbers of qubits to large-scale quantum computers. When envisaging a large quantum network, or ultimately the quantum internet, many different implementations of an edge will be needed, e.g., to reliably connect close-by units composing a single computation node, different types of nodes, as well as distant nodes.

Two promising research avenues for the scalability of quantum networks are in the development of *distributed* and *hybrid* quantum communication and computation technologies. The utility of distributed quantum technologies lies in the likely scenario that it is easier to connect many high-functioning, modestly sized, often homogeneous, devices (which have been demonstrated), using quantum effects like entanglement as a resource, than to scale a single device to have the same net processing power [4–10]. A complementary means of scaling quantum networks is by developing a hybrid quantum architecture, where either [11] different types of (i) qubits or (ii) nodes are connected so that tasks can be delegated so as to leverage the strengths of a given type of qubit or node.

Case (i) can be envisaged as a hybrid device that uses different kinds of qubits for different purposes. For instance, using separate types of qubits for local logic operations and for interfacing with quantum channels, which would allow for communication between nodes with minimal disruption to local computation or storage processes [12–17]. In case (ii), heterogeneous nodes (or smaller intranodal units), that are based on different quantum technologies, are connected to form the elementary unit of a hybrid quantum network (or node). Such hybridization would be valuable in making more powerful large-scale nodes, say a node that integrates solid-state computation units leveraging fast nanosecond gates (at the expense of relatively short microsecond coherence times for both depolarization and dephasing) [18–21] with atom-based memory units with long coherence times on the order of milliseconds (or seconds for ions though they can be significantly longer [22], typically limited by dephasing times) at the expense of slower microsecond gate times [23–25] for hybrid quantum computation [26–28]. More broadly, realizing such hybrid links would increase the connectivity of quantum networks. Especially as different technologies (trapped ions, superconducting circuits, etc.) become better established as platforms for qubit implementation, how to interface them is an important question to address [29–38].

A. Background and scope

The implementation of a specific edge depends on the properties of the nodes it is linking, including their underlying technological implementation, natural energy scale, physical separation, and intended function (say communication or computation). In this work we focus on discrete (as opposed to

[*]Contact author: krandles@uoregon.edu
[†]Contact author: svanenk@uoregon.edu

continuous [39]) variable quantum communication in which intermediate "flying qubits" carry quantum information along an edge realized by a guided quantum channel. Photons are the quintessential flying qubit, and the one we consider here (though phonons could be used, e.g., in some optomechanical systems [40–42] and other solid-state systems [43]), as they can efficiently travel between nodes and they have several degrees of freedom (mode occupation number, polarization, temporal-mode, etc.) that can be used to encode quantum information.

We focus on a guided channel (e.g., optical fiber [6,23,44,45] or microwave coaxial cable [46–53]) linking close-by nodes, say within a given laboratory or device, leaving the consideration of nonguided free-space channels to other work [54–58]. The main issue with distant nodes is that the fidelity of states being transferred (and likewise the degree of entanglement generated) typically decreases exponentially with the length of the connecting channel due to photon absorption and noise in the channel (the rate of this decay can be minimized by using telecom light) [59–62]. In principle, this issue can be solved using a quantum repeater, which itself needs to be able to distribute entanglement between close-by "repeater stations," though further details are beyond the scope of this work [63–65]. Accordingly, we will not explicitly address the difficulties of connecting distant nodes. Note that the error correction protocols we mention are still relevant for distant nodes though they will have more overhead for larger distances.

In this paper we focus on the theoretical implementation of a deterministic quantum state transfer (QST) scheme capable of linking hybrid quantum nodes [in the sense of case (ii) above] via itinerant photons. In particular, we consider connecting two different types of spatially separated nodes, with potentially different spectral properties (resonance frequency and decay width). The state of a qubit prepared at the "sender" node 1 is mapped to the state of an emitted photon wave packet (facilitated by local controls) that is sent to a "receiver" node 2 via a guided channel. To optimally be absorbed at node 2, and hence to map the photonic state to a material qubit state, this wave packet must be modified, tailoring its time-frequency shape [66]. In our previous work [67] we showed how this can be accomplished by incorporating a unitary transformation, U, that time reverses [see Supplemental Material (SM) [68] Sec. A4 for some discussion of why we emphasize time reversal], frequency shifts, and stretches or compresses the intermediate photon wave packet along the quantum channel [69]. The original version of this scheme (without the unitary) was proposed in the seminal work of Cirac and co-workers [70]. In the time domain, U is given by

$$U(t,t') = \sqrt{\xi} e^{i\omega_0(T-t)} \delta(t' - \xi(T-t)). \tag{1}$$

With the inclusion of this unitary transformation, we showed how to design system controls (laser pulses) that will transfer the state of a qubit at node 1 to one at node 2 even if the nodes have significantly different resonance frequencies and decay rates (provided we can implement U correctly). This is especially important in hybrid cases, where without U the likelihood of node 2 absorbing a photon emitted by node 1, even for well-designed controls, is very small. A schematic representation of how such a pair of linked nodes might fit into a larger quantum network is given in Fig. 1.

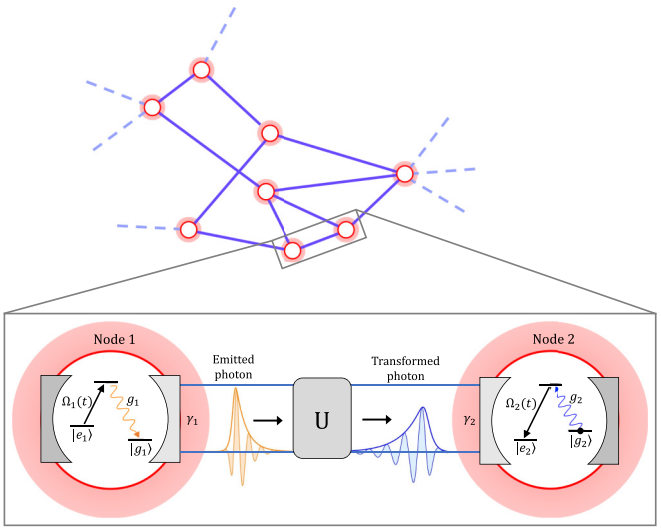

FIG. 1. Potential subgraph representing part of a quantum network (above) with a zoomed in focus (below) on two nodes (red points) and the quantum channel (blue edges) linking them, along which our QST scheme is implemented (see the main text for details). The graph structure is only for illustration purposes, showing how our scheme can fit into the bigger picture of quantum networking. The dashed lines indicate potential continuations of the network to other nodes. The lower image is modified from figures of Refs. [70] and [67].

In this paper we consider and analyze realistic errors that can occur in the hybrid QST scheme of our previous work [67], which demonstrated how the scheme works in ideal conditions. We focus on errors in the implementation of the unitary transformation, as other common errors, such as those due to photon absorption in the transmission line, incorrect laser controls, and cavity loss, are well known and understood [71–75]. This lets us show our protocol's utility in the presence of these realistic errors especially when it is supplemented by known error correction protocols [74,75] that can correct these common errors as well as errors in the unitary transformation using local quantum computations with auxiliary quantum emitters at each node (see Sec. III D). Nonetheless, error mitigation remains a crucial part of making such error correction protocols viable, specifically to keep the expected number of repetitions of a primitive transfer operation low and moreover to lessen additional overhead.

We also show that the probability of successfully transferring the state from one node to another, P_{success}, is determined (rather intuitively) by the overlap between the actual and ideal single-photon wave packets to be incident on node 2 denoted by Ψ and Φ, respectively. Specifically, we find

$$\boxed{P_{\text{success}} = |\langle\Phi|\Psi\rangle|^2 = \left|\int_{-\infty}^{\infty} dt\, \Phi^*(t)\Psi(t)\right|^2} \tag{2}$$

(see Sec. III A for the corresponding derivation in the particular case we focus on in this work, where each node is comprised of a three-level atom in a cavity, and see

SM Sec. A for a general argument for this result, which ultimately amounts to the Born rule). This can be understood by interpreting the successful completion of the protocol as a photodetection event in which the receiving node can be thought of as a photodetector, that (in the case of a "click") would project onto a particular single-photon wave packet Φ, which is determined by the parameters of node 2 and the laser driving it.

B. Outline

We outline the model for the interaction of the nodes and present our QST scheme in Sec. II. This includes specifying the corresponding Hamiltonian and equations of motion (EOMs) for the amplitudes of various excitations as well as giving an overview of the standard errors present in such a scheme. In Sec. III we consider errors in the unitary transformation. In Sec. III A we show how these errors can be described in the context of quantum measurement theory in terms of positive operator-valued measures (POVMs). Then in Sec. III B we show how the ideal value of the unitary transformation's timing parameter can be determined and in Sec. III C we perform some further numerical analysis of the probability of successful state transfer in the presence of unitary errors. In Sec. III D we highlight how known error correction protocols could be used to reliably perform this state transfer procedure in the presence of realistic errors. In Sec. III E we consider the relevance of our work in heralded schemes, as opposed to deterministic schemes. Finally, in Sec. IV we discuss the utility of our scheme and provide an outlook of other contexts where it could be employed. Additional analysis and supporting details regarding the scope of our results are provided in the Supplemental Material (SM) for this paper [68].

II. SCHEME AND MODEL

Here we summarize the model used for two linked nodes of a quantum network interacting via a quantum channel. For brevity, we leave much of the corresponding derivations and further details to Refs. [76,77], the textbook [78], and our previous work [67]. Starting from the Gardiner-Collett model [76], one can show that in the quantum trajectory formalism [77], the dynamics (during time intervals when no quantum jump occurs) are determined by an effective non-Hermitian Hamiltonian of the form

$$H_{\text{eff}} = H_1 + H_2 + H_{\text{tl}}. \tag{3}$$

Here H_j is the Hamiltonian for node $j = 1, 2$ and H_{tl} accounts for the nodes' interaction via the *transmission line*.

A. Node implementation

Here we consider nodes that can encode the state of a qubit in an effective two-level system with a controllable coupling to a well-defined electromagnetic field mode. Such a node is readily realized, at least theoretically, by a three-level Λ-type atom (or ion) in a high-Q optical cavity [70] and there has been significant recent experimental progress in such systems [13,79–81] (see Sec. II F). Accordingly, we focus on this case (both here and in our previous work [67]) as an exemplar of the physics underlying our scheme. The overall scheme applies more generally so our use of "atom" throughout the paper can often be mapped to other material systems such as an ionic, solid-state, or superconducting qubit in analogous setups. These atomic systems along with the rest of our QST scheme are highlighted in Fig. 1. In this case, at each node the state of a qubit is encoded in the ground states of the atom, $|e\rangle$ and $|g\rangle$, which are coupled via a Raman transition through an auxiliary atomic excited state $|r\rangle$. We consider asymmetric cavities that preferentially couple to the transmission line, e.g., by using a partially transmitting mirror to interface with the transmission line and a (near) perfectly reflective outer mirror.

That is, the dynamics of the first Raman qubit are controlled using a laser pulse that drives a transition from $|e_1\rangle$ to $|r_1\rangle$, which is followed by the transition $|r_1\rangle$ to $|g_1\rangle$ and the emission of a photon into cavity 1, and meanwhile leaves $|g_1\rangle$ undisturbed with no corresponding emission. Thus, if atom 1 was in the "excited" state $|e_1\rangle$, an emitted photon would leak out of cavity 1, propagate down the transmission line along which it would be transformed via U, before its incidence on node 2. Then atom 2, which is prepared in $|g_2\rangle$, can simply undergo the Raman process analogous to that undergone by atom 1 but in the backwards order, with the goal of inducing absorption of the photon. This is possible as by implementing U we have effectively equalized the spectral properties of the two nodes (analogous to impedance matching).

By linearity, this process can thus be used to implement our QST scheme, where the state of atom 1, $c_g|g_1\rangle + c_e|e_1\rangle$, is transferred to the photon, $c_g|0\rangle + c_e|1\rangle$, and then to atom 2, $c_g|g_2\rangle + c_e|e_2\rangle$. Here we take the photonic qubit to be encoded in the occupation number degree of freedom, i.e., either the vacuum $|0\rangle$ or single-photon $|1\rangle$ state in a certain mode [82,83]. Other encodings could potentially be used with appropriate modifications to our scheme. There are of course tradeoffs between different encodings, e.g., the polarization encoding $\{|H\rangle, |V\rangle\}$ is more robust in some scenarios [84,85] yet the occupation number encoding is necessary for the known error correction protocols we consider (see SM Secs. A6 and D for further discussion).

For these nodes, the effective dynamics in the single (or zero) excitation subspace are ultimately determined by the Hamiltonian ($\hbar = 1$) [67,70]

$$H_j = iG_j(t)(a_j^\dagger|g_j\rangle\langle e_j| - a_j|e_j\rangle\langle g_j|). \tag{4}$$

The operators $a_j^\dagger$ and a_j are the creation and annihilation operators for cavity j, respectively. Likewise $|e_j\rangle\langle g_j|$ and $|g_j\rangle\langle e_j|$ are the raising and lowering operators for the effective two-level atom j, respectively. Here $G_j(t) = g_j\Omega_j(t)/2\Delta_j$ is the Jaynes-Cummings interaction strength between the effective two-level atom and cavity at node j, where (as depicted in Fig. 1) g_j is the bare atom cavity coupling, $\Omega_j(t)$ is the user-controlled Rabi frequency envelope of the driving laser, and $\Delta_j = \omega_{Lj} - \omega_{rj}$ is the laser detuning. Note $G_j(t)$ is real with the implicit time-dependent laser phase, of the form $e^{i\phi_j(t)}$, factored out. To obtain this form for H_j we selected specific laser frequencies ω_{Lj} to eliminate shifts to the cavity energy states and chose the laser phases $\phi_j(t)$ (the chirps specifically) to compensate for the ac Stark shift to $|e_j\rangle$ [see Eq. (34) of Ref. [67] and the surrounding discussion for details as well

as SM Sec. B1]. Additionally, we assumed far off-resonant driving lasers (to suppress spontaneous emission [86]) so that we could adiabatically eliminate the excited states $|r_j\rangle$, and we went into a rotating frame at the frequency of the laser driving each system ω_{Lj} (in which the states $|e\rangle$ and $|g\rangle$ are to be interpreted).

B. Interaction model

Assuming a vacuum field input, or less strictly that no light is incident on the nodes in relevant modes, the connection of the nodes is ultimately described by [67]

$$H_{\rm tl} = -\frac{i}{2}(\gamma_1 a_1^\dagger a_1 + \gamma_2 a_2^\dagger a_2 + 2\sqrt{\gamma_1\gamma_2}e^{i\zeta t}a_2^\dagger \tilde{a}_1), \tag{5}$$

which provides an effective description of the transmission line in which node 2 is effectively directly coupled to the transformed output of node 1. This is accounted for by the operator $\tilde{a}_1$, which is an annihilation operator for the transformed photon that exits the unitary transformation device. Note that both a_1 and $\tilde{a}_1$ are time-delayed operators, which implicitly account for the time delay of light propagating between the nodes. This description highlights the role of the transmission line as an intermediary for the transfer of excitations from node 1 to node 2 (via the $a_2^\dagger\tilde{a}_1$ term). Here γ_j is the decay rate for cavity j into the transmission line. The relative phase of $\zeta = \omega_{L2} - \omega_{L1}$ in the excitation transfer term corresponds to oscillations at the mismatch in the frequencies of the lasers driving the two systems and is due to going into the aforementioned rotating frames for each node.

Within this model we assume the coupling to be unidirectional with photons only propagating from system 1 to 2 (there is no $a_2 a_1^\dagger$ term in $H_{\rm tl}$), at least during the QST procedure. Ideally, this unidirectionality should be a consequence of atom 2 being prepared in a stable ground state $|g_2\rangle$, yet it can be physically imposed as necessary, e.g., by using a circulator [87]. Then U does not affect system 1 dynamics and a_1 acts in the Heisenberg picture in a standard way, i.e., on $|C\rangle_1 = c_0|0\rangle_1 + c_1|1\rangle_1$ it acts as

$${}_1\langle 0|a_1(t)|C\rangle_1 = c_1(t). \tag{6}$$

Meanwhile, in this effective description, the second system is effectively directly coupled to the *unitarily transformed* output of system 1. This is accounted for by the $a_2^\dagger\tilde{a}_1$ term of Eq. (5), where $\tilde{a}_1$ encodes the effect of U, acting as

$${}_1\langle 0|\tilde{a}_1(t)|C\rangle_1 = \chi(t)c_1(f(t)) \tag{7}$$

in contrast to Eq. (6), where [88]

$$\chi(t) = \begin{cases} 0, & t_i < t < t_s, \\ \sqrt{\xi}e^{i\omega_0(T-t)}, & t_s < t < t_f, \\ 1, & \text{otherwise} \end{cases} \tag{8}$$

and

$$f(t) = \begin{cases} \text{undefined}, & t_i < t < t_s, \\ \xi(T-t), & t_s < t < t_f, \\ t, & \text{otherwise}. \end{cases} \tag{9}$$

Here t_s is the time at which the transformed field starts to be produced and it is controlled via the relation $T = t_s(1 + 1/\xi)$. These functions are broken up into intervals as the part of the photon wave packet to be transformed, taken to be of duration $t_l = l/c$, must pass through the unitary transformation device (in the time interval $t_i \equiv t_s - t_l < t < t_s$), before the transformed wave packet is produced (in the interval $t_s < t < t_f \equiv t_s + t_l/\xi$). Outside of the time interval where the transformation is happening $\tilde{a}_1$ reduces to the standard a_1. The form of these functions for $t_s < t < t_f$ comes directly from Eq. (1), assuming that the untransformed pulse is blocked at the transformation device during the production of the transformed field. [This assumption is not necessary, but it leads to a simpler description of how the unitary transformation's effect can be encoded in the time argument of a fictitious system $\tilde{1}$ that is, effectively, directly driving system 2 (see Ref. [67] for further discussion). Furthermore, the distinction of whether we block the original field for $t_s < t < t_f$ does not matter if the two Raman processes are driven by lasers with substantially different frequencies $|\zeta| = |\omega_{L2} - \omega_{L1}| \gg \gamma_{1,2}$ (see Sec. III B)]. The crucial part is that the transformed part of the field (which should be the entirety of the single-photon wave packet assuming the control parameters are suitably picked and implemented) has the time-reversed and stretched argument $\xi(T - t)$.

C. Model generality

Importantly, our focus on a particular kind of node does not limit the scope of our work, which is meant to concern hybrid links, as the ideas behind our scheme apply to many other analogous controllable systems that could be used for either (or both) node(s). In fact, the Hamiltonian governing the system dynamics we analyze [given in Eqs. (3)–(5)] is quite general for deterministic QST schemes like ours, so the physics should be identical after an appropriate mapping of physical parameters. This is provided the unitary transformation U can be implemented to transduce the intermediate photon between the emitting and receiving nodes energy and time scales. [Note that U has a proposed implementation in the optical regime [89]. In other regimes, say for microwave systems or hybrid cases, such as the coupling of microwave and optical nodes, some aspects of such a transformation have been considered yet to our knowledge the entire unitary we consider has not been (see SM Sec. A5 for further discussion)].

In particular, we assume that we utilize nodes for which individual excitations can controllably and reversibly be transferred from the material system to a photonic mode (emission) and vice versa (absorption), often at the single-photon level, say mediated by a cavity or resonator [70,85,90]. It should then be possible to recast the Hamiltonians for the nodes themselves into the standard Jaynes-Cummings form [as was done for Eq. (4)] through the appropriate adiabatic elimination of auxiliary states, selection of unitary transformations to the node Hamiltonian, and tuning of the system and control parameters. One benefit of such coherent and reversible interactions is that you can generate different kinds of target states, e.g., tune the wave packet's shape, amplitude, and phase (see SM Sec. B for further discussion). This is to be contrasted against heralded, probabilistic approaches such as those based on spontaneous emission (see Sec. III E). The form of the Hamiltonian describing the

coupling of the nodes, Eq. (5), is also common within the context of input-output theory in which one eliminates the channel from the description (via its corresponding continuous mode field operators) to obtain a simpler description where the two nodes are effectively directly coupled (see SM Sec. A2 for further details and examples).

D. System evolution

Starting from Eq. (3), the zero-excitation ground state evolves trivially $|gg\rangle|00\rangle \to |gg\rangle|00\rangle$ as

$$i\frac{d}{dt}|gg\rangle|00\rangle = H_{\text{eff}}|gg\rangle|00\rangle = 0 \tag{10}$$

in the interaction picture. Meanwhile the dynamics of a state in the single-excitation subspace

$$\begin{aligned}|\psi(t)\rangle =& \alpha_1(t)|eg\rangle|00\rangle + \alpha_2(t)|ge\rangle|00\rangle \\ &+ \beta_1(t)|gg\rangle|10\rangle + \beta_2(t)|gg\rangle|01\rangle\end{aligned} \tag{11}$$

are encoded by α_j and β_j, which are the state amplitudes for an excitation being in atom j ($|e_j\rangle$) and cavity j ($|1_j\rangle$), respectively. The corresponding amplitude EOMs are

$$\dot{\alpha}_1 = -G_1\beta_1, \tag{12a}$$

$$\dot{\beta}_1 = G_1\alpha_1 - \frac{\gamma_1}{2}\beta_1, \tag{12b}$$

$$\dot{\alpha}_2 = -G_2\beta_2, \tag{12c}$$

$$\dot{\beta}_2 = G_2\alpha_2 - \frac{\gamma_2}{2}\beta_2 - \sqrt{\gamma_2}e^{i\zeta t}\Psi(t), \tag{12d}$$

where

$$\begin{aligned}\Psi(t) :=& \sqrt{\gamma_1}\chi(t)\beta_1(f(t)) \\ \approx& \sqrt{\gamma_1\xi}e^{i\omega_0(T-t)}\beta_1(\xi(T-t)),\end{aligned} \tag{13}$$

is the transformed wave packet (as we are working in a rotating frame, it is a slowly varying envelope function [91]) emitted by system 1 that is driving system 2. The approximation in Eq. (13) is exact during the transformed field production $t_s < t < t_f$ and hence holds in the large l limit. Note that by tuning the laser frequencies and phases to obtain the simple Jaynes-Cummings type node Hamiltonians of Eq. (4) we are fixing α_1 and β_1 to have the same constant phase, so without loss of generality we take them both to be real. This simplified case, where we tune the control parameters so that the system 1 amplitudes are real, is of course not general, though it entirely suffices for our QST scheme and makes our analysis easier. It is worth mentioning that one can controllably modulate the phase of the emitted photon wave packet, $\Psi(t) = \sqrt{\gamma_1}\beta_1(t)$, in time by adjusting the parameters of the driving laser, namely the phase (though this can exacerbate non-Markovian effects, which need more careful treatment [92]), and then α_1 also acquires a time-dependent phase (see SM Sec. B1 for more details).

Note that in our setup the transfer $|g_1\rangle \to |g_2\rangle$ happens by default [see Eq. (10)], and so the principal goal is to transfer any excitation from the first qubit to the second, $|e_1\rangle \to |e_2\rangle$. Thus, in the single-excitation subspace, we want $|\alpha_1(t \to -\infty)| = 1$ and $|\alpha_2(t \to \infty)| = 1$; the former condition is satisfied via appropriate local state preparation while the latter requires the transmission process to be implemented correctly. Accordingly, we deem the probability of successful QST to be $P_{\text{success}} \equiv |\alpha_2(t \to \infty)|^2$, with the caveat that one need also transfer the relative phase of the qubit states, which requires an interferometrically stable channel (see the discussion at the end of Sec. III A for further details).

E. Simplified treatment

As we have alluded to, we want to highlight the role of the unitary transformation U in our QST scheme. Accordingly, we use several simplifying strategies that allow us to set aside other well known kinds of errors and quantify the impact of U by the single parameter P_{success}. In this subsection, we list these strategies and briefly discuss how they can naturally be incorporated into our analysis (see SM Sec. D1 for further details). These strategies include that

(1) emission of the Λ system into modes other than the desired cavity mode is treated *post hoc*,

(2) cavity field loss into modes other the relevant transmission line mode is treated *post hoc*,

(3) transmission line loss is treated *post hoc*,

(4) we assume the laser pulses (or other control drives) are implemented correctly, and

(5) we do not account for dispersion in the transmission line.

Strategies (1) and (2) are worded for the emission process from node 1, yet we likewise (due to time-reversal symmetry) apply them during absorption at node 2.

The *post hoc* treatment in strategies (1), (2), and (3) is performed by multiplying our probability of success by the respective survival probabilities P_1, P_2, and P_3 of the photon being transferred to the desired mode during emission into (or absorption out of) the cavity (see SM Sec. B3), the cavity-channel interactions, and its propagation through the channel [79,93,94]. That is, the evolution described in Sec. II D is conditioned on attempts where the photon is not lost (absorbed or in an orthogonal mode). Thus, the modified success probability of our scheme is

$$\tilde{P}_{\text{success}} = P_1 \times P_2 \times P_3 \times P_{\text{success}}. \tag{14}$$

One can naturally separate the first two survival probabilities into contributions from each of the individual nodes. Namely, letting $\mathcal{P}_{\text{em-}j}$ and $\mathcal{P}_{\text{cav-}j}$ denote the respective probabilities of the emitter and cavity at node j coupling to the desired mode (which are the same for emission and absorption due to time-reversal symmetry), we have $P_1 = \mathcal{P}_{\text{em-1}}\mathcal{P}_{\text{em-2}}$ and $P_2 = \mathcal{P}_{\text{cav-1}}\mathcal{P}_{\text{cav-2}}$.

As an instructive example, here we consider the case where nodes 1 and 2 undergo the same amount of loss. In particular, we take $\mathcal{P}_{\text{em-1}} = \mathcal{P}_{\text{em-2}} = C_{\text{em}}/(1 + C_{\text{em}})$ and $\mathcal{P}_{\text{cav-1}} = \mathcal{P}_{\text{cav-2}} = C_{\text{cav}}/(1 + C_{\text{cav}})$. Here C_{em} and C_{cav} are cooperativity parameters that quantify how well the emitters and cavities, respectively, are able to produce photons in the desired output mode. Meanwhile, for strategy (3), we consider exponential transmission line loss $P_3 = e^{-x/x_{\text{tl}}}$ with attenuation distance x_{tl} [95]. (See SM Sec. D1 for further explanation and motivation of these parameters and the corresponding survival probabilities; realistic values are given in Sec. II F.) In this

case, we have

$$\tilde{P}_{\text{success}} = P_{\text{success}} \times \left(\frac{C_{\text{em}}}{1+C_{\text{em}}} \frac{C_{\text{cav}}}{1+C_{\text{cav}}} \right)^2 e^{-x/x_{\text{tl}}}. \quad (15)$$

Strategies (4) and (5) are used for simplicity and could be accounted for implicitly via modifications to the actual and target wave packet shapes Ψ and Φ in P_{success} of Eq. (2). Strategy (4) is well founded in that laser errors in the amplitudes G_j and phases ϕ_j are typically negligible compared to the other errors we consider, yet such errors could easily be included in our model and numerics if necessary. One point of note that is obfuscated by the effective treatment of Eq. (5) is the role of the relative timing of the laser pulses (which is implicitly encoded in the time-delayed operators for node 1). A relative timing error of δt would result in P_{success} being determined by the overlap of $\Psi(t+\delta t)$, instead of $\Psi(t)$, with the target $\Phi(t)$, degrading the excitation transfer. Thus, in strategy (4), we additionally assume that no such relative timing errors are made, which demands care, but can be accomplished by characterizing and controlling the photon propagation time through the channel and using a common reference clock for both nodes. In regards to strategy (5), distortion to the wave packet Ψ induced by channel dispersion can be (partially) compensated for by modifying the control pulses [92] as well as the unitary transformation U (see SM Sec. A4). However, the comprehensive modeling and treatment of such distortion effects is beyond the scope of our work. We note that channel dispersion poses less of a problem when using short channels and/or small bandwidth (large duration) photons, making strategy (5) more justified in these cases.

F. Realizable parameters in cavity QED experiments

We will now consider realistic values of the parameters $C_{\text{em}}, C_{\text{cav}}$, and x_{tl} for atom or ion in an optical cavity type nodes. This allows us to quantify the impacts of the standard loss mechanisms that we set aside in the previous subsection. For transmission line loss we consider two cases that are employed or sought in the literature: optical and telecom light, for which $x_{\text{tl}}^{(\text{opt})} \approx 1.2$–$1.5$ km and $x_{\text{tl}}^{(\text{tele})} \approx 15$–$25$ km, respectively [96]. For emitter and cavity losses, we consider several references that use nodes similar to our exemplar case and in Table I we list the corresponding cooperativities and survival probabilities they are (or would be) able to achieve. The average cooperativities based on this table are $C_{\text{em}}^{(\text{avg})} = 9.0$ and $C_{\text{cav}}^{(\text{avg})} = 5.9$, whereas, if the maximum and minimum values are disregarded in each case, the averages become 3.6 and 5.8, respectively.

We note that the reported ion experiments tend to have lower emitter and cavity cooperativities than the neutral atom experiments. One main reason for this is that small mode volumes are needed to obtain large ion-light couplings g, yet they also result in a stronger disturbance to the trapping field due to stray fields caused by charge build up on the dielectric mirrors in a typical Fabry-Perot type cavity setup. This can be largely circumvented using a fiber-based Fabry-Perot cavity, in which the two cavity mirrors are each an end face of an optical fiber, wherein the accumulated charge is distributed over the fibers' dielectric surfaces [97]. In Sec. III D we use these realistic x_{tl} values and the tabulated cooperativity values to inform how implementable our scheme is (in consonance with an error correction protocol) in different parameter regimes (see Fig. 7).

TABLE I. Overview of realizable emitter and cavity parameter values based on several recent experimental analyses that consider nodes comprised of a neutral atom or ion coupled to an optical cavity (in experiments that use two such nodes, we list the values for each, labeled A and B). Here we list the emitter and cavity cooperativities (C_{em} and C_{cav}) as well as the corresponding maximum probabilities that a photon is emitted by the atom or ion into the correct cavity mode, $\mathcal{P}_{\text{em}} = C_{\text{em}}/(1+C_{\text{em}})$, and then from the cavity into the desired output mode (in the transmission line), $\mathcal{P}_{\text{cav}} = C_{\text{cav}}/(1+C_{\text{cav}})$. In some references, C_{cav} was not given and could not be calculated directly, yet an analog to $\mathcal{P}_{\text{cav}}$ is reported. In these cases we infer the values of C_{cav} by backtracking (indicated via italics). Here $P_{\text{tot}} = P_1 P_2 = (\mathcal{P}_{\text{em}}\mathcal{P}_{\text{cav}})^2$ is the combined probability of this full emission process at node 1 and symmetrically of absorption at node 2, assuming both nodes have the same cooperativities. The emitter in each of the neutral atom experiments is a ^{87}Rb atom. In the trapped ion experiments, Refs. [103] and [104] use a single $^{174}\text{Yb}^+$ ion and up to 5 $^{40}\text{Ca}^+$ ions, respectively, while the others [80,97] use a single $^{40}\text{Ca}^+$ ion. An extended version of this table is given in SM Sec. D1.

Emitter type	Refs.	C_{em}	$\mathcal{P}_{\text{em}}$ (%)	C_{cav}	$\mathcal{P}_{\text{cav}}$ (%)	P_{tot} (%)
Neutral atom	[98]	2.8	74	*9.0*	*90*	44
	[99,100]	6.0	86	11.9	92	62
	[101]	66.7	99	1.3	57	31
	[94]	2.9	75	8.0	89	44
	[102] A	7.7	89	11.5	92	66
	[102] B	6.9	87	6.0	86	56
Ion	[103]	0.05	5	0.5	32	0.02
	[79,104]	0.3	24	*6.7*	*87*	4
	[80] A	0.8	45	*0.3*	*20*	0.8
	[80] B	1.9	66	*3.5*	*78*	26
	[97]	3.2	76	0.3	2[a]	2

[a]The setup of Ref. [97] is not intended to preferentially produce photons out of one mirror. Accordingly, the cavity parameter values reported here appear small (and are excluded from the reported $C_{\text{cav}}^{(\text{avg})}$) yet they could readily be increased by modifying the setup.

III. UNITARY ERRORS

Here we consider errors in the unitary parameter values of ω_0, ξ, and T. We focus on cases where the transformation duration, t_l, is long enough to transform essentially all of the pulse. That is, we do not analyze errors due to the unitary not being implemented for long enough, which (at least in nonlinear optical setups) could be due to not using a long enough medium for the transformation device. Errors such as photon absorption or distortion can be corrected for [74,75], though the corresponding protocols do not correct for errors due to the undesired production of a photon. Hence we assume there is no other mechanism for atom 2 to absorb an excitation, which is consistent with the assumption of a vacuum field input to system 1 needed to obtain the effective Hamiltonian of Eq. (3). In particular, we assume that there are no relevant thermal excitations, which is only valid for systems at low temperatures relative to their operation frequency such that

the average thermal occupation number $\bar{n}_{\rm th} = 1/(e^{\hbar\omega/k_BT} - 1)$ is nearly zero (it is desirable to have it be far less than 1) [105]. This is typically a very good approximation for optical systems though systems that operate at lower frequencies need to be cooled. For instance, at room temperature $T = 293$ K optical light with wavelength $\lambda \approx 700$ nm will have $\bar{n}_{\rm th} \approx 3 \times 10^{-31}$, whereas microwave light with $\lambda \approx 20$ mm will have $\bar{n}_{\rm th} \approx 400$. Hence adequate cooling is crucial in reducing thermal noise and loss experienced by guided microwave channels such as cryogenic microwave links [53,106].

The ideal values of the frequency and stretching parameters are $\omega_0 = \omega_{0i} \equiv \zeta = \omega_{L2} - \omega_{L1}$, which compensates for the difference in frequencies of the two systems, and $\xi = \xi_i \equiv \gamma_2/\gamma_1$, which stretches the wave packet to match the receiving timescale of cavity 2 [67]. Unlike for ω_0 and ξ, there is not a similarly "nice" expression for the ideal value of the timing parameter $T = t_s(1 + 1/\xi)$, which controls the starting time for the transformation t_s. However, the goal is simple: for a given l one need simply select a t_s (and hence T) such that the largest contributions to $\beta_1(t)$ are transformed. We can be more precise in finding the optimal value of T, though we defer this to Sec. III B, where the analysis will be made easier using the machinery we will develop in the following section. For now we simply note that such an optimal T, which we will call T^*, must exist.

As we are focusing on errors in the unitary parameters in this section, we assume that G_1 is implemented correctly such that α_1, β_1 are as desired (see SM Sec. B for a discussion of how an appropriate α_1 or β_1 can be used to determine the corresponding G_1) and that [107]

$$G_2(t) = \xi_i G_1(\xi_i(T_i - t)) \tag{16}$$

with $T_i = T|_{\xi=\xi_i}$ [see strategy (4) above]. Note that with this choice, the laser phase $\phi_2(t)$ for system 2 is also time reversed and scaled relative to that for system 1, assuming they are implemented in the prescribed way. Hence the second laser pulse is not affected by an error in the unitaries' values of ξ and T. (In fact T_i need not take on its optimal value T_i^* as long as it is consistent in U and G_2 and l is long enough for the entire wave packet to be transformed.) One can show that the above choices for the unitary parameters and G_2's relation to G_1 are an optimum, in that given solutions α_1 and β_1, there are corresponding solutions for system 2,

$$\alpha_2^i(t) = e^{i\omega_{0i}T_i}\alpha_1(\xi_i(T_i - t)) \tag{17}$$

and

$$\beta_2^i(t) = -e^{i\omega_{0i}T_i}\beta_1(\xi_i(T_i - t)) \tag{18}$$

(assuming l is long enough for the entire wave packet to be transformed), which act in a time-reversed manner relative to their system 1 counterparts. Hence, with the above choices and assumptions, if atom 1 loses an excitation, α_1 goes from one to zero, then atom 2 will absorb it, as $|\alpha_2^i|$ goes from zero to one.

A. Unitary parameter errors

If an excitation is sent from atom 1, we want atom 2 to absorb it and hence to achieve $|\alpha_2(t \to \infty)| = 1$. Thus, we analyze here the structure of α_2's EOM, which, after eliminating β_2 in the coupled Eqs. (12c) and (12d), can be found to be

$$\ddot{\alpha}_2 = \left(\frac{\dot{G}_2}{G_2} - \frac{\gamma_2}{2}\right)\dot{\alpha}_2 - G_2^2\alpha_2 + \sqrt{\gamma_2}e^{i\zeta t}G_2\Psi(t). \tag{19}$$

Rearranging the terms, it follows that

$$L(t)\alpha_2(t) = \Psi(t) \tag{20}$$

with

$$L(t) := \frac{e^{-i\zeta t}}{\sqrt{\gamma_2}G_2}\left[\frac{d^2}{dt^2} - \left(\frac{\dot{G}_2}{G_2} - \frac{\gamma_2}{2}\right)\frac{d}{dt} + G_2^2\right] \tag{21}$$

a linear operator (we *assume* it is invertible), and so it has some Green's function $\Gamma^*(t, t')$ [108] such that

$$\alpha_2(t) = \int_{-\infty}^{\infty} dt'\,\Gamma^*(t, t')\Psi(t'). \tag{22}$$

Here we treat $\Psi(t)$ as some generic (possibly subnormalized) wave packet of arbitrary shape. This is justified mathematically as, in terms of the differential equation Eq. (20), $\Psi(t)$ is just some nonhomogeneous source term, and the Green's function solution is indifferent to the origin of Ψ. Note we cannot design the first laser pulse G_1 (even if it is supplemented by our unitary) to produce arbitrary wave packets from system 1 (see SM Sec. B5 for further discussion).

We will now use this Green's function to derive an expression for the limiting value of α_2 at some *end* time t_e by which the amplitudes have reached steady values (in practice t_e can be taken to be $+\infty$ mathematically). Physically, we know that $|\alpha_2| \leqslant 1$, so with the shorthand $\Gamma(t = t_e, t') = \Gamma_e(t')$ we have

$$1 \geqslant |\alpha_2(t_e)|^2 = \left|\int_{-\infty}^{\infty} dt'\,\Gamma_e^*(t')\Psi(t')\right|^2 = |\langle\Gamma_e|\Psi\rangle|^2, \tag{23}$$

where we are assuming Γ_e is well defined and unique (in practice, this is typically the case with appropriate boundary conditions, and our numerics in Sec. III C substantiate the validity of the solution we find), yet we do not yet know its norm. [We focus on $\Gamma_e(t')$ because our primary goal is that the excitation is ultimately transferred (as part of the QST scheme), not to know the exact dynamics of the excitations. Accordingly, we do not attempt to compute $\Gamma(t, t')$ for all times t, though we do note that it must be causal so $\Gamma(t, t' > t) = 0$.] This is true for arbitrary Ψ, which will be normalized (in the single-excitation subspace) unless there are losses, say due to photon absorption. Thus, we can select

$$|\Psi\rangle = \frac{|\Gamma_e\rangle}{\sqrt{\langle\Gamma_e|\Gamma_e\rangle}} \tag{24}$$

(up to a phase) to maximize $|\alpha_2(t_e)|^2 = |\langle\Gamma_e|\Psi\rangle|^2$ via the Cauchy-Schwarz inequality. With this selection, by Eq. (23) we have

$$1 \geqslant |\alpha_2(t_e)|^2 = |\sqrt{\langle\Gamma_e|\Gamma_e\rangle}|^2 = \langle\Gamma_e|\Gamma_e\rangle \tag{25}$$

so $|\Gamma_e\rangle$ is either a normalized or subnormalized quantum state.

We know that with ideal parameters $\omega_0 = \omega_{0i}$ and $\xi = \xi_i$ (again, for sufficiently long l with appropriate timing $T = T_i$)

our unitary will produce the ideal wave packet

$$\Phi(t) = \Psi(t)|_{\omega_0=\omega_{0i},\xi=\xi_i,T=T_i,l\to\infty} = \sqrt{\gamma_2}e^{i\omega_{0i}(T_i-t)}\beta_1(\xi_i(T_i-t)), \tag{26}$$

which evidently is the time-reversed, stretched, and frequency shifted counterpart of the wave packet to be emitted by system 1. Crucially, note that for properly designed α_1 that start at 1 at some early *preparation* time t_p, from Eq. (17) we have $|\alpha_2^i(t=t_e)| = |e^{i\omega_{0i}T_i}| = 1$ for $t_e \geqslant T_i - t_p/\xi_i$ and hence the corresponding normalized $\Phi(t)$, $\langle\Phi|\Phi\rangle = 1$, would lead to perfect absorption at system 2 [109]. Thus, again using Cauchy-Schwarz, we have that

$$1 = \left|\alpha_2^i(t_e)\right|^2 = |\langle\Gamma_e|\Phi\rangle|^2 \leqslant \langle\Gamma_e|\Gamma_e\rangle\langle\Phi|\Phi\rangle = \langle\Gamma_e|\Gamma_e\rangle \leqslant 1, \tag{27}$$

where we used Eq. (25) in the last step. It clearly follows that

$$\langle\Gamma_e|\Gamma_e\rangle \equiv 1 \tag{28}$$

and hence $|\Gamma_e\rangle$ corresponds to a normalized state vector, and moreover

$$|\Gamma_e\rangle = |\Phi\rangle \Longleftrightarrow \Gamma_e(t) = \Phi(t) \tag{29}$$

(again, up to a phase) as the states must be linearly dependent to saturate Cauchy-Schwarz.

It thus follows that the probability of success is

$$P_{\text{success}} \equiv |\alpha_2(t_e)|^2 = |\langle\Phi|\Psi\rangle|^2 = \left|\int_{-\infty}^{\infty} dt'\, \Phi^*(t')\Psi(t')\right|^2 \tag{30}$$

as claimed in Eq. (2). That is, the probability of success is given by the squared overlap of the incident photon wave packet $\Psi(t)$ with the ideal wave packet $\Phi(t)$. Thus, if no errors occur, the transformed wave packet $\Psi(t)$ will be equal to the normalized $\Phi(t)$ and hence $P_{\text{success}} = 1$. It follows that system 2 can be thought of as a photodetector that in the case of a click would project on the ideal state via the POVM element

$$\hat{\Pi}_{\text{success}} = |\Phi\rangle\langle\Phi|. \tag{31}$$

Note we would only register such a click (or not) if we appended an atomic measurement of the receiving qubit state. Then, we see that, for the pure input state $\rho_{\text{in}} = |\Psi\rangle\langle\Psi|$,

$$P_{\text{success}} = \text{Tr}(\rho_{\text{in}}\hat{\Pi}_{\text{success}}) = |\langle\Phi|\Psi\rangle|^2, \tag{32}$$

which matches Eq. (30). Note that this does not assume that Ψ is normalized; it could be subnormalized due to an error at system 1, an error in the unitary, or loss during the transformation.

More generally, such a POVM would be a weighted sum of projectors (mixed) but here it is a lone projector (pure) as our process is reversible. For instance, if the system parameters, such as g_j, varied due to fluctuations in the position of the atoms or cavities, then averaging over these fluctuations would give a mixed POVM [110]. Another relevant situation would be fluctuations in the unitary transformation parameters (ω_0, ξ, and T), which would result in the input state ρ_{in} of Eq. (32) being an incoherent mixture of states Ψ with different parameters according to some underlying classical probability distribution. Specifically, if there is classical uncertainty or variation in the unitary transformation parameters, e.g., variation in ω_0 due to the finite linewidth of a control laser, then the actual probability of success would be $P_{\text{success}}(\omega_0, \xi, T)$ averaged over the corresponding classical probability distribution. Note that the ideal wave packet should remain the same as it is purely determined by the parameters of node 2 and the laser driving it, G_2.

Note that P_{success} is actually just the probability that an excitation from atom 1 is transferred, via the intermediate photonic degree of freedom, to atom 2. This assumes that no other excitations that can excite atom 2 are produced during the transmission. We additionally assume that the phase of the initial state of atom 1 is correctly transferred to atom 2, i.e., the channel needs to be interferometrically stable [13,82,83]. This can be accomplished using stable local oscillators as frequency references at each system to establish a common phase reference for both nodes. Then phase stabilization techniques can be used to maintain (and control) the phase induced by the channel, which is easier for shorter channels [67,82,83,111,112]. We assume such considerations are taken so we can focus on the impact of U rather the examination of such phase errors. Even if such phase errors do occur, error correction protocols could be used to eliminate them (see Sec. III D). We will proceed under these assumptions so that P_{success}, as defined in Eq. (30), is a good measure of the success of the entire QST scheme. Note that what "success" ultimately means is up to the particular scheme. For instance, the quantum state fidelity $\mathcal{F}$ may be a more apt measure of successful QST. Here $\mathcal{F}$ is given by the magnitude squared of the overlap of the initial (qubit) state of atom 1 with the final state of atom 2. Notably in the absence of phase errors $\mathcal{F}(|c_e|)$ is bounded below by $P_{\text{success}} = |\alpha_2(t_e)|^2$ (see SM Sec. A3 for details).

B. Optimal timing

Now that we have shown this new perspective, where system 2 can be thought of as a single-photon detector, we will derive an expression that the optimal unitary timing parameter T^* must satisfy. (Note this is new within the context of this problem; that POVMs play a key role in describing photodetection [113–118] and measurements more generally [119–121] is well known.) We compute T^* assuming that the transformation is implemented correctly in all ways except that it has a limited duration t_l. Then the probability of success based on the Green's function argument above is

$$P_{\text{success}}(t_s) = |\langle\Phi|\Phi_l\rangle|^2, \tag{33}$$

where $\Phi_l(t) = \Psi(t)|_{\omega_0=\omega_{0i},\xi=\xi_i,T=T_i}$ is the actual transformed wave packet for some finite l, assuming the ideal frequency and stretching parameters as well as consistent timing; $\Phi_l(t)$ is equal to $\Phi(t)$ for $t_s < t < t_f$. Maximizing $P_{\text{success}}(t_s)$ can thus be accomplished by solving for the t_s (and hence T_i) such that

$$\frac{d}{dt_s}P_{\text{success}}(t_s) = 0 \tag{34}$$

(and verifying that the optimum is a maximum).

Note that

$$\langle\Phi|\Phi_l\rangle = \sqrt{\gamma_1\gamma_2}\int_{-\infty}^{\infty} dt\,[e^{-i\zeta(T_i-t)}\beta_1(\xi_i(T_i-t))\chi(t)\beta_1(f(t))], \tag{35}$$

where $\chi(t)$ and $f(t)$ characterize the different stages of the transformation and are implicitly evaluated at $\omega_0 = \omega_{0i}$, $\xi = \xi_i$, and $T = T_i$ here. The parameters T_i, t_i, and t_f (which are related to the different stages) all implicitly depend on t_s and so Eq. (34) should be solved numerically in general. However, in typical cases the contribution to Eq. (35) due to the untransformed portion of the wave packet (i.e., outside the interval $t_s < t < t_f$) will be negligible. This is due to some combination of l being long enough for the β_1 product in the integrand to be small over the relevant domain and the term being far off-resonant, with $|\omega_{0i}| \gg \gamma_{1,2}$, such that the phase rapidly oscillates and the integrand averages to zero. In such a case, effectively none of the untransformed wave packet emitted from system 1 will induce a transition at system 2 and so we have

$$\begin{aligned}\langle\Phi|\Phi_l\rangle &\approx \int_{t_s}^{t_f} dt\,|\Phi(t)|^2 \\ &= \gamma_2\int_{t_s}^{t_f} dt\,\beta_1^2(\xi_i(T_i-t)) \\ &= \gamma_1\int_{t_i}^{t_s} dt\,\beta_1^2(t)\end{aligned} \tag{36}$$

(the approximation gets better for large $|\omega_{0i}|$ and/or l). As this inner product is real, we can maximize $P_{\text{success}}(t_s)$ by finding the t_s such that

$$0 = \frac{d}{dt_s}\int_{t_s-t_l}^{t_s} dt\,\beta_1^2(t) = \beta_1^2(t_s) - \beta_1^2(t_s-t_l). \tag{37}$$

This is a much simpler condition than in the general case and it can easily be solved for numerically once G_1 is specified and hence β_1 is determined. The corresponding solution is the ideal value of t_s, which we will denote by $t_s^* \equiv T_i^*/(1+1/\xi_i)$.

C. Numerical results

To makes plots illustrating errors in the different unitary parameters, we must specify the first laser pulse G_1. A natural case to consider is the G_1 such that the amplitude for atom 1, α_1, logistically decreases from 1 to 0:

$$\alpha_1(t) = \frac{1+\tanh(-kt)}{2}. \tag{38}$$

Note, for any monotonically decreasing α_1, one can compute the corresponding laser pulse G_1 that would generate it [see Eq. (B7) of SM Sec. B2]. Then the amplitude for cavity 1 can be determined as $\beta_1 = -\dot{\alpha}_1/G_1$, which in turn gives the exact form of the ideal emitted photon wave packet Φ of Eq. (26). (See SM Sec. B2 for β_1 in this logistic α_1 case.) We can thus compute how errors in the unitary transformation parameters, i.e., incorrect values of ω_0, ξ, and T, degrade the transfer resulting in a decreased P_{success}. The impact of such errors on P_{success} can be seen graphically as in Fig. 2, where we compare a wave packet Ψ due to a unitary transformation with stretching and timing errors to the corresponding ideal wave packet Φ.

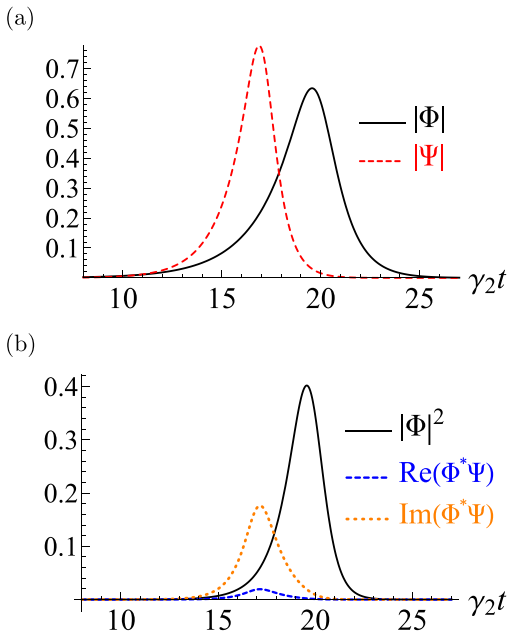

FIG. 2. (a) Plot of the ideal wave packet modulus $|\Phi|$ for $k = 2$, with the unitary parameters taking on their ideal values $\omega_0 = \omega_{0i} = 50$, $\xi = \xi_i = 1/2$, $T = T_i^* = 19.7$ for transformation duration $t_l = 10$, and a nonideal wave packet modulus $|\Psi|$ still with $\omega_0 = \omega_{0i}$, but with stretching and timing errors $\xi = 0.75$ and $T = 17$. (All quantities are in units where $\gamma_2 = 1$.) (b) Plot of the integrand in Eq. (30) for computing P_{success} in the ideal case (solid line) and the real and imaginary parts in the nonideal case (dashed and dotted lines, respectively). Here, for visualization purposes, we decompose Eq. (30) as $P_{\text{success}} = [\int dt\,\mathrm{Re}(\Phi^*\Psi)]^2 + [\int dt\,\mathrm{Im}(\Phi^*\Psi)]^2 = 0.186$, whereas $P_{\text{success}} = \int dt|\Phi|^2 = 1$ for the ideal wave packet (which assumes the entirety of the wave packet emitted from node 1 is transformed).

Furthermore, we can compute how P_{success} varies as a function of the amount of error in the various transformation parameters. For instance, we illustrate the effect of errors in the unitary parameters ω_0, T, and ξ by plotting P_{success} versus one of these parameters, assuming the other parameters are ideal in Figs. 3–5, respectively. We work with a set of shifted "error variables" that are centered at zero: $\Delta\omega_0 \equiv \omega_0 - \omega_{0i}$, $\Delta\ell_\xi \equiv \log_2\xi - \log_2\xi_i$, and $\Delta T \equiv T - T_i^*$. We consider the logarithm of ξ in most of our plots as its ideal value is a ratio of two decay widths, $\xi_i = \gamma_2/\gamma_1$, so errors in ξ should scale multiplicatively, e.g., doubling ξ (with respect to its ideal value) should be (about) as bad as halving it. In each of these plots (Figs. 3–5), the solid black lines are a cubic interpolation between 201 points with the independent variable's values distributed evenly over the intervals shown. The corresponding value of P_{success} is given by the overlap calculation $|\langle\Phi|\Psi\rangle|^2$. The overlaid colored points are calculated by numerically solving the coupled ordinary differential equations (ODEs) of Eqs. (12a)–(12d) for various values of the independent variable (with larger separations because the relevant numerics are more computationally expensive).

For concreteness we focus on the specific case of a logistic α_1 with $k = 2$ and the physical parameters $\omega_{0i} = 50$ and $\xi_i = 1/2$. Additionally, we assume a long transformation length $l = 10$, for which $T^* = 19.7$, such that, in the absence

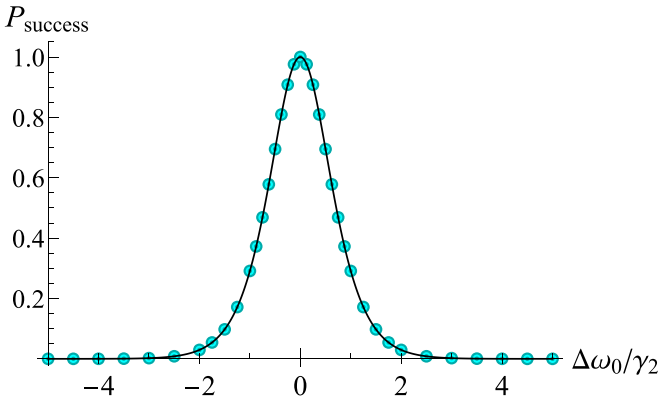

FIG. 3. Plot of P_{success} as a function of the detuning $\Delta\omega_0$, assuming the other unitary parameters are ideal. We take the underlying parameter values to be the same as in Fig. 2 (that is, $k = 2$, $\omega_{0i} = 50$, $\xi_i = 1/2$, and $t_l = 10$ in units where $\gamma_2 = 1$). The probability of success quickly falls off away from resonance, $\Delta\omega_0 = 0$. The solid line is from a state overlap calculation using Eq. (30) and the overlaid points are from directly numerically solving coupled EOMs for the state amplitudes (see main text).

of errors in the unitary, effectively all of the wave packet would be transformed with $P_{\text{success}} = 0.999\,995 \approx 1$. Here all quantities are given in natural units in which $\gamma_2 = c = 1$. Importantly, these underlying parameter values are not crucial as, at least for large l as we have here, only the error variables (made dimensionless with appropriate factors of γ_2) and the wave packet shape (as effectively controlled by α_1) matter (see SM Sec. C). Hence the results gleaned from this specific case apply more generally. The largest discrepancy in calculating P_{success} between the original coupled ODEs solution method and the POVM wave packet overlap method is 1.1×10^{-6}, which we assume to be numerical error (in particular, we see that this specific error value goes down if we increase our error tolerance when solving the ODEs). Hence this numerical comparison serves as a strong indicator of the validity of the POVM based results we found.

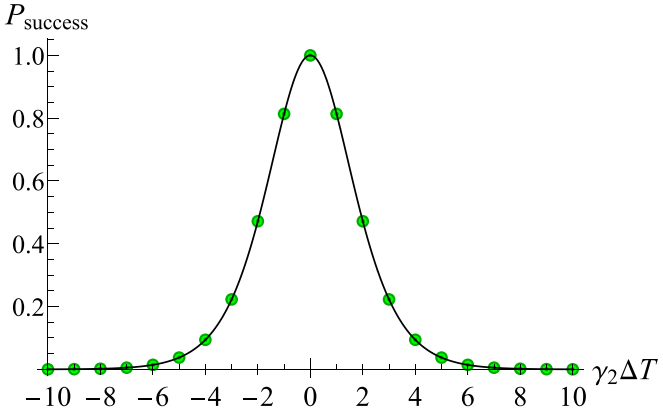

FIG. 4. Plot of P_{success} versus ΔT assuming the other unitary parameters are ideal (with the same underlying physical parameters as the previous figures). The solid line is from an overlap calculation and the overlaid points are from solving coupled amplitude EOMs (see main text).

The probability of success quickly falls off away from its peak value near unity as ω_0, T, and ξ are shifted from their ideal values. The narrow peak around $\omega_0 = \omega_{0i}$ in Fig. 3, which has a full width at half maximum (FWHM) of $1.4\gamma_2$, illustrates the importance of frequency conversion. We note that the shape and width of the P_{success} versus ω_0 curve do not change appreciably as the central frequency $|\omega_{0i}|$ is further increased. This is because, as alluded to above, only the detuning of the transformed wave packet from resonance with system 2 relative to γ_2, $|\Delta\omega_0|/\gamma_2$, significantly matters during the transformation. Moreover, for large $|\omega_{0i}|$ the untransformed portions of the wave packet will not induce an excitation in atom 2. Thus, even when $|\omega_{0i}|$ is very large, e.g., $|\omega_{0i}|/\gamma_2 \sim 10^6$ is typical, the FWHM will be stable. Here it remains at $1.4\gamma_2$ (for this logistic α_1 with $k = 2\gamma_2 = \gamma_1$), and hence it is critical to control against frequency errors. Note that wave packets with narrower temporal shapes are less susceptible to such frequency errors, though this will be limited by emitting node parameters (see SM Sec. B4).

The couplings γ_j tend to be on the order of kHz-MHz, and are typically smaller in the microwave regime as compared to the optical. Hence, typical values of γ_j can vary by 2 to 3 orders of magnitude between different systems and so $\xi_i = \gamma_2/\gamma_1 \sim 100$–$1000$ is reasonable for hybrid interconnects (assuming $\gamma_2 > \gamma_1$, otherwise ξ_i would be the reciprocal of this). Experiments across different platforms have demonstrated the ability to shape photon wave packets, which includes stretching and compression by these orders of magnitude [94,122–124]. Note that the results for different ξ_i can be mapped between one another because, as mentioned above, P_{success} is predominantly determined by the error variables, $\Delta\ell_\xi$ in this case. Importantly, the seemingly narrow width of P_{success} as a function of $\Delta\omega_0/\gamma_2$ does not doom us as sub-kHz-MHz level precision in frequencies (necessary to obtain $|\Delta\omega_0| \lesssim \gamma_2$) is possible using standard, tunable, narrow-linewidth lasers [125–128], as well as mid-infrared and terahertz laser sources based on difference frequency generation [129,130].

We can quantify how much two of the dimensionless error variables $\{\Delta\omega_0/\gamma_2, \Delta\ell_\xi, \gamma_2\Delta T\}$ depend on one another by computing their "index of separability" $\mathcal{S}$ [131]. For an $m \times n$ matrix A we define $\mathcal{S}$ in terms of its singular values $\{\sigma_i(A)\}$ with maximum $\sigma_{\max}(A)$ as

$$\mathcal{S}(A) := \frac{\sigma_{\max}^2(A)}{\sum_i \sigma_i^2(A)}, \tag{39}$$

which is the square of the ratio of the induced 2-norm and Frobenius norm of A. This index of separability is bounded as $0 < 1/\min\{m, n\} \leqslant \mathcal{S}(A) \leqslant 1$, where the maximum $\mathcal{S}(A) = 1$ entails that A is separable, i.e., can be written as an outer product of two vectors, and the minimum $\mathcal{S}(A) = 1/\min\{m, n\}$ (which is nearly zero for large matrices) entails that A is full rank with all equal singular values. However, practically the smallest observed values will be much larger than this (∼0.75 here), which comes from comparing to random matrices (see SM Sec. C).

For instance, with the same underlying physical parameters as in Figs. 2–5, we take the joint probability distribution for $\gamma_2\Delta T$ and $\Delta\ell_\xi$ assuming ω_0 takes on its ideal value, $P_{\text{success}}(\Delta T, \Delta\ell_\xi)|_{\omega_0=\omega_{0i}}$, compute it on a grid of equally

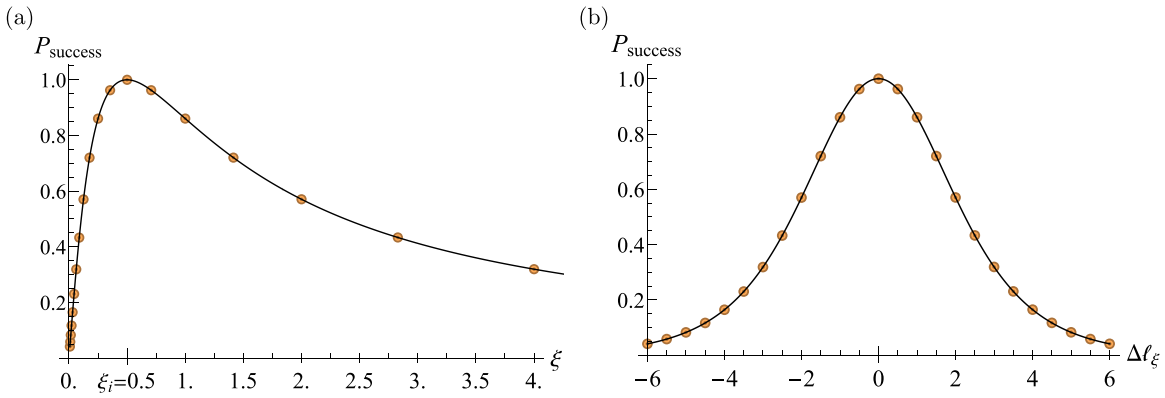

FIG. 5. Plots of P_{success} versus ξ on (a) a linear scale and (b) a logarithmic scale with $\Delta\ell_\xi = \log_2 \xi/\xi_i$, assuming the other unitary parameters are ideal (with the same underlying physical parameters as the previous figures). The solid line is from an overlap calculation and the overlaid points are from solving coupled amplitude EOMs (see main text).

spaced values for ΔT and $\Delta\ell_\xi$ yielding a matrix, and then compute its index of separability to be

$$S_{T,\xi} \equiv \mathcal{S}\big[P_{\text{success}}(\Delta T, \Delta\ell_\xi)|_{\omega_0=\omega_{0i}}\big] = 0.87. \tag{40}$$

Similarly, for the other two variable pairs (keeping the third variable at its ideal value) we find

$$S_{\omega_0,\xi} \equiv \mathcal{S}[P_{\text{success}}(\Delta\omega_0, \Delta\ell_\xi)|_{T=T^*}] = 0.87 \tag{41}$$

and

$$S_{\omega_0,T} \equiv \mathcal{S}[P_{\text{success}}(\Delta\omega_0, \Delta T)|_{\xi=\xi_i}] = 0.998. \tag{42}$$

[Each of these $\mathcal{S}$ values is computed on a 121 by 121 grid (matrix) with the same spacings as described in the Fig. 6 caption over a rectangular region twice as large in each direction as those depicted. These reported values ultimately serve as upper bounds for the separability index for large grids. Corresponding lower bounds can be calculated using the zero-mean counterparts of the P_{success} matrices used here, yielding respective $\mathcal{S}$ values of 0.80, 0.80, and 0.97 compared to Eqs. (40)–(42). (See SM Sec. C for additional method details.)]

Hence ω_0 and T errors are largely independent of one another (as the corresponding probability distribution is almost separable, $\mathcal{S} \approx 1$), whereas errors in ω_0 and T are distinctly dependent on what ξ error occurs. The corresponding joint probability distributions are given in Fig. 6 and can be used to get visual intuition for the index of separability. For instance, Fig. 6(a) illustrates that errors in T and ξ are dependent on each other, which can intuitively be explained as wave packet timing errors in T will reduce the overlap, yet there will be relatively more overlap if one also elongates the wave packet in the time domain by choosing $\xi < \xi_i$ ($\Delta\ell_\xi < 0$). This analysis accounts for dependencies of the errors on one another that are intrinsic to our model. We leave considerations of other error dependencies that may be due to a particular implementation of the transformation U to other work.

D. Error correction

We have highlighted many things can go wrong in the implementation of the unitary itself, which is in addition to standard errors due to incorrect driving laser pulses, incorrect

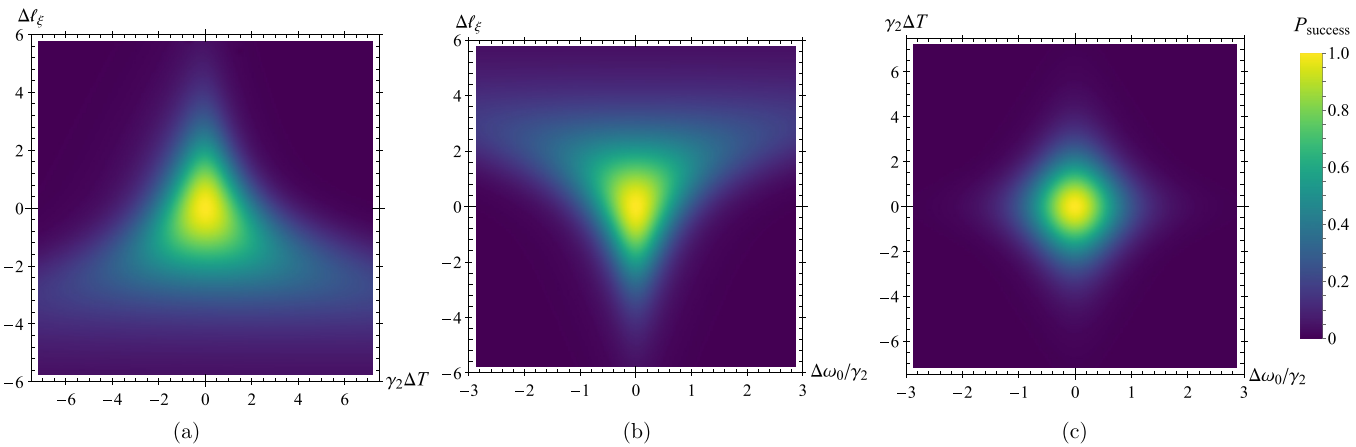

FIG. 6. Density plot of P_{success} as a function the error variable pairs for the transformation parameters (a) T and ξ, (b) ω_0 and ξ, and (c) ω_0 and T assuming the other unitary parameter is ideal (with the same underlying physical parameters as the previous figures). Each plot is computed as the cubic interpolation of a 61 by 61 grid of points that are evenly spaced over the region shown and is colored according to the legend.

laser frequencies, fluctuating system parameters, as well as photon absorption or other losses in the transmission line, cavities, material qubits, or transformation device. With all of these possibilities, the presence of errors on a single attempt of a QST scheme like ours is inescapable, though crucially we can correct for these errors. Accordingly, we will now discuss the applicability of a few error correction protocols to our scheme as well as their limitations.

1. ECZ protocols

By using the occupation number encoding our scheme could naturally be improved by utilizing one of two relatively low overhead error correction protocols [74,75] that capitalize on the feasibility of suppressing photon production errors $|0\rangle \to |1\rangle$. We refer to these as the "ECZ protocols" after their authors' last names. These protocols can correct for photon loss and phase errors, which are recurrent in standard transmission lines, e.g., optical fibers and waveguides. They do so using auxiliary quantum emitters, again envisaged as atoms in a cavity, that can encode the state of a qubit at each node and serve as a form of redundancy. They cannot correct for errors caused by the creation of photons in the relevant mode, which is often reasonable as the production of photons can be suppressed in a well-isolated setup operating at an appropriate temperature (such that there is low thermal occupation, $\bar{n}_{\text{th}} \ll 1$, which as previously discussed is more of a problem in microwave-based systems).

Each ECZ protocol is based on repeating a certain primitive transfer operation, which we will refer to as a trial, that includes 1 or 2 QST attempts (typically 2), local single-qubit and two-qubit entanglement gate operations, and measurements of auxiliary qubits or states. These local gate and measurement operations are assumed to be implemented perfectly, though in practice these operations will also be error prone and hence limit how close to unity the ultimate transfer fidelity can be. In the earlier protocol [74], measurements are performed on each trial, a successful outcome of which validates the state transfer. In the later protocol [75], a given trial serves as a "purification" step to be iterated so that a target state is approached exponentially, at a rate that gets faster for smaller net errors in the protocol, and hence can be reached up to some error threshold in fidelity. (See SM Sec. D for further discussion of these protocols.)

Both ECZ protocols consider an effective channel in which on a single transmission attempt (which forms an integral part of both protocols) the initial state will evolve for large times (so that no excitations remain in the cavities) according to a map of the form [132]

$$\begin{matrix} |g_1\rangle|g_2\rangle \\ |e_1\rangle|g_2\rangle \end{matrix} \longrightarrow \begin{matrix} \alpha|g_1\rangle|g_2\rangle \\ \beta|g_1\rangle|e_2\rangle + \Upsilon_1|g_1\rangle|g_2\rangle + \Upsilon_2|e_1\rangle|g_2\rangle, \end{matrix} \tag{43}$$

where α, β, and $\Upsilon_{1,2}$ are constants. These are the form of the long time limit of the solutions to EOMs analogous to Eq. (12) with $|\beta| = |\alpha_2(t_e)|$ and $|\Upsilon_2| = |\alpha_1(t_e)|$, but with additional possible errors included. Importantly for our scheme, *an error in the unitary transformation falls under this class of channel* as it will contribute to photon loss. Chiefly, an incorrectly shaped incident wave packet will not be absorbed by node 2 and hence will be directed out a different spatial mode [87]. This is in addition to loss due to absorption at the transformation device. Such errors can be accounted for via the amplitudes β and Υ_1. Thus, our scheme can naturally be incorporated as an extended version of the transmission steps in the ECZ protocols, which can aptly be utilized in our context for reliable QST between hybrid nodes.

We acknowledge that such a protocol would slow down the rate of entanglement generation due to the time it takes to repeat the primitive transfer scheme as well as to perform the requisite local computations. Importantly, however, if we can achieve reasonably small error probabilities in the necessary operations the slowdown in rate can be manageable. We will now illustrate this by considering the expected number of repetitions $E[n]$ of the earlier ECZ protocol (until success) [74] in the case where $|\alpha| = 1$, as we have previously assumed in our scheme, yet its phase could be nontrivial due to a relative phase error (see SM Sec. D2). Consider an error on a given transmission of $|\Upsilon_1|^2 + |\Upsilon_2|^2 = \varepsilon$ such that $|\beta|^2 = 1 - \varepsilon$ by normalization. In this model the worst case, that with the largest $E[n]$, is when we are dominated by Υ_1 errors (i.e., $|\Upsilon_1|^2 = \varepsilon$ and $\Upsilon_2 = 0$). In this worst case we find

$$E[n] = \frac{4}{(1-\varepsilon)(2-\varepsilon)^2}, \tag{44}$$

which starts at 1 for $\varepsilon = 0$, corresponding to only needing a single trial without errors, and monotonically increases as a function of $\varepsilon \in [0, 1]$, tending towards $+\infty$ as $\varepsilon \to 1$ as the state transfer entirely fails for $\beta = 0$ (see SM Sec. D for the general derivation and further details). Note in fact we expect to be in this regime, $|\Upsilon_1| \gg |\Upsilon_2|$, with photon loss and unitary transformation errors being dominant such that

$$\varepsilon \approx |\Upsilon_1|^2 \approx 1 - \tilde{P}_{\text{success}}; \tag{45}$$

see Eq. (14). In Fig. 7 we use Eqs. (44) and (45) to show how $E[n]$ depends on the bare P_{success} value with the inclusion of realistic standard errors (informed by the parameter values of Table I). Knowing the dependence of $E[n]$ on P_{success} for experimentally achievable parameter regimes can inform how much unitary transformation loss or error (quantified by P_{success}) can be tolerated in a given implementation. Importantly, we find that if small unitary transformation error probabilities, $1 - P_{\text{success}}$, can be achieved, then few trials (protocol repetitions) will typically be needed when linking nodes with good (yet realizable) cooperativities linked by relatively short channels (e.g., with lengths around an order of magnitude smaller than the attenuation distance x_{tl} or less).

2. Alternate protocols and their scope

Depending on the achievable $E[n]$, the magnitude of errors in the local operations needed for the ECZ protocols, and other implementation details, the employment of another correction protocol or even a nondeterministic heralded approach may be appropriate (see Sec. III E). There are several alternate error correction protocols that can be used for deterministic quantum communication via photons. For consistency, here we focus on protocols that use the mode occupation number encoding (see SM Sec. A6 for a discussion of other encodings). Such protocols can be realized using multiphoton states as a type of redundancy, e.g., using so-called binomial [133]

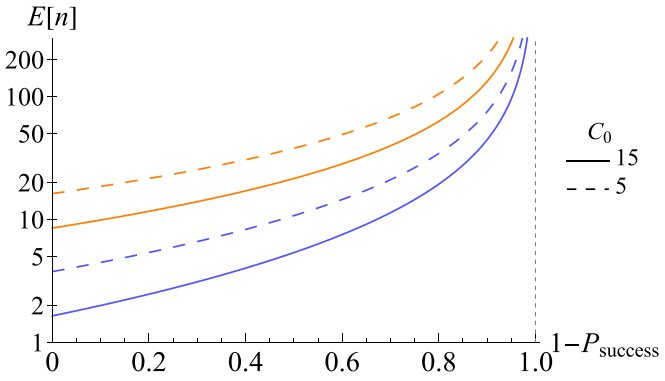

FIG. 7. Plot of the expected number of ECZ [74] error correction trials, $E[n]$ from Eq. (44), on a logarithmic scale versus the error in the itinerant photon's temporal-frequency shape, $1 - P_{\text{success}}$. This is done for realistic cooperativities informed by the values listed in Table I. Here for simplicity we take $C_{\text{em}} = C_{\text{cav}} = C_0$, as in both cases currently achievable cooperativity values are around $C_0 = 5$ (dashed lines), while $C_0 = 15$ (solid lines) is more optimistic yet plausible. These plotted cases could equivalently represent other cooperativity pairs with the same respective combined probabilities $P_{\text{tot}} = P_1 P_2$ of 48% and 78%. For each C_0 value, we consider two cases: no transmission loss ($x/x_{\text{tl}} = 0$, $P_3 = 1$) and transmission loss over one attenuation distance ($x/x_{\text{tl}} = 1$, $P_3 = 1/e \approx 37\%$), which are shown in the lower (blue online) and upper (orange online) lines, respectively, for a given line type (solid or dashed). See Sec. II F for standard values of x_{tl} for optical and telecom light in fiber. As P_{success} gets small, tending towards zero ($\varepsilon \to 1$), the expected number of trials quickly grows, diverging like $1/P_{\text{success}}$ to leading order (indicated via the dashed vertical asymptote). For instance, $E[n]$ reaches 10 when $\varepsilon \approx 0.75$, which in the above cases with cooperativities of 15 and 5 corresponds to bare P_{success} values of about 33% and 53%, respectively, for $x/x_{\text{tl}} = 0$.

or cat [52] codes, or using photonic graph states (such as cluster states) generated from a single emitter [134–136]. Each of these alternate protocols comes with their own technical challenges, especially in hybrid interfacing contexts like ours where we would need to transform all the itinerant photons in a logical state preserving way. Moreover, both the sender and receiver would need to be able to interface with these multiphoton logical states. For instance, such binomial codes are realizable with superconducting circuit technology [47] but are more challenging for other implementations with less control of the requisite multiphoton states. Similarly, only a few emitters, including quantum dots and atoms in cavities, have demonstrated viability in the generation of such photonic graph states. Accordingly, one advantage of the ECZ protocols, especially for hybrid interconnects, is their relative simplicity as the generation of single photon states is a standard, feasible task for a wide variety of node implementations.

To make such protocols (including those of ECZ) applicable in the NISQ (noisy intermediate-scale quantum [137]) era with error prone operations on small numbers of qubits one has to compromise between the potential noise reduction of a given error correction protocol versus the realistic "cost" of its implementation in a given deterministic QST proposal or experiment. This cost includes additional resources such as local operations and controls as well as auxiliary emitters that can simultaneously be coupled at each node, which all come with their own potential errors as well as slower rates. For instance, when adapted to our hybrid case, the earlier ECZ protocol [74] is contingent on the errors in the unitary parameters, laser pulses, and system parameters [specifically α and β in Eq. (43)] being consistent between subsequent transmissions in a given trial. If this systematic condition breaks down, then the later ECZ protocol [75] should potentially be used as it can iteratively purify more general random errors in the channel even with potentially non-Markovian decoherence. However, this more comprehensive nature of the later protocol is at the expense of additional overhead, in the form of additional local operations, especially for large errors, so a compromise must be made.

E. Relevance in heralded schemes

At this point, it is useful to contrast our deterministic scheme against commonly employed heralded schemes for QST and/or remote entanglement generation. Here we give the basic idea of such heralded schemes and discuss how the ideas underlying our work can be applied to them. Such a heralded scheme may be appropriate if the ECZ or alternate error correction protocols discussed above for a deterministic scheme are not realizable (see SM Sec. A7 for some discussion of the pros and cons of deterministic versus heralded schemes). In many such schemes [80,82,83,138–140], two nodes each emit a photon that encodes the state of a qubit in one of its degrees of freedom (typically using a polarization encoding). Said photonic qubits states are (ideally) maximally entangled to their emitter's qubit state. Then a photonic Bell-state measurement is implemented in which the two photons interfere at a 50:50 beam splitter and a subsequent coincident detection of photons with orthogonal qubit states ideally heralds the creation of a remote entangled state between the matter qubits at each node, otherwise the procedure is repeated until success.

The quality of the generated remote entanglement is ultimately determined by how indistinguishable the two photons are, whose states we denote by $|\psi_A\rangle$ and $|\psi_B\rangle$. Namely, the fidelity of the remote entangled state relative to a target maximally entangled state is determined by the mode overlap of the two photons $\mathcal{C} \equiv \langle\psi_A|\psi_B\rangle$ as [138]

$$\mathcal{F} = \frac{1 + |\mathcal{C}|^2}{2} \tag{46}$$

(note this ignores detector background counts and imperfect emitter-photon entanglement, which will further degrade $\mathcal{F}$ [80]). The key physics behind this is that for indistinguishable photons, $|\mathcal{C}| = 1$, the beam splitter removes which-path information leading to the entanglement swapping from the emitter-photon pairs to the emitters with unit fidelity (after an appropriate heralded measurement). Meanwhile, the interference of distinguishable photons at the beam splitter results in the addition of a classical mixture to the otherwise entangled (heralded) joint state of the emitter qubits. This combination preserves the joint state populations yet reduces the coherences, thereby lowering the state fidelity (i.e., it is a two-qubit dephasing channel).

Thus, having nearly indistinguishable photons as inputs to the photonic Bell-state measurement of such a heralded scheme is crucial for obtaining high fidelity remote entanglement. This can be connected to our work in that a transformation like our U (but without time reversal) could be used to make the photons emitted by heterogeneous nodes nearly indistinguishable and thus to achieve heralded hybrid remote entanglement generation (or QST via an additional quantum teleportation step). Moreover, the analysis of the errors in such a transformation, to be employed in a heralded scheme, carries over almost directly from our work with $|\mathcal{C}|^2$ effectively replacing P_{success} as a figure of merit for the success of the scheme.

IV. DISCUSSION

In this paper we have demonstrated theoretically how unitary transformations to the temporal-spectral mode of a photon serving as a flying qubit between hybrid quantum nodes can be used to drastically improve the probability of successfully transferring quantum information between the nodes. We showed that the probability of transferring an excitation from one node to another, which is a good measure of successful quantum state transfer, is given by the modulus squared of the overlap of the spectral shapes of the actual and ideal photon wave packets. Doing so makes the role of the unitary transformation apparent: it should transform the emitted photon to one with this ideal spectral shape (which can be calculated). Importantly, our scheme applies quite generally to any nodes in which controlled quantum light-matter interaction can be realized to reversibly transfer the state of a material qubit to a photonic degree of freedom and back, not just for the type of nodes we focus on, i.e., a three-level atom in a cavity.

We analyzed the impact of errors in the implementation of the unitary transformation. This includes showing how the success of the protocol depends on the deviations from the ideal parameters as well as quantifying how much these parameter errors depend on one another. This analysis, along with our considerations of more standard errors, can be used to determine what kinds of errors dominate in a given physical setup, say to form an error budget. Furthermore, we discussed how our scheme can naturally be incorporated with and aid known error correction protocols to significantly suppress or potentially eliminate unavoidable errors in deterministic quantum state transfer, even between hybrid systems. Such an error-corrected adaptation of our scheme could be used to distribute entanglement in a quantum network or for distributed quantum computing. As a next step, our methods could be applied to other material systems and the unitary transformation's physical implementation could be further considered, especially for cases outside of the optical regime.

[1] H. J. Kimble, The quantum internet, Nature (London) **453**, 1023 (2008).

[2] S. Wehner, D. Elkouss, and R. Hanson, Quantum internet: A vision for the road ahead, Science **362**, eaam9288 (2018).

[3] A. Sadhu, M. A. Somayajula, K. Horodecki, and S. Das, Practical limitations on robustness and scalability of quantum internet, arXiv:2308.12739.

[4] L. K. Grover, Quantum telecomputation, arXiv:quant-ph/9704012.

[5] J. I. Cirac, A. K. Ekert, S. F. Huelga, and C. Macchiavello, Distributed quantum computation over noisy channels, Phys. Rev. A **59**, 4249 (1999).

[6] A. Serafini, S. Mancini, and S. Bose, Distributed quantum computation via optical fibers, Phys. Rev. Lett. **96**, 010503 (2006).

[7] L. Jiang, J. M. Taylor, A. S. Sørensen, and M. D. Lukin, Distributed quantum computation based on small quantum registers, Phys. Rev. A **76**, 062323 (2007).

[8] C. Monroe and J. Kim, Scaling the ion trap quantum processor, Science **339**, 1164 (2013).

[9] R. Beals, S. Brierley, O. Gray, A. W. Harrow, S. Kutin, N. Linden, D. Shepherd, and M. Stather, Efficient distributed quantum computing, Proc. R. Soc. A **469**, 20120686 (2013).

[10] R. Van Meter and S. J. Devitt, The path to scalable distributed quantum computing, Computer **49**, 31 (2016).

[11] We limit our usage of "hybrid quantum" to these cases, though the phrase is used more broadly, e.g., to indicate hybrid classical-quantum technologies or hybrid continuous-discrete variable systems. Alternatively, our use of "hybrid" in discussing differing types of systems and nodes of a quantum network could be replaced by "heterogeneous" to be contrasted with homogeneous implementations connecting like systems.

[12] C. B. Young, A. Safari, P. Huft, J. Zhang, E. Oh, R. Chinnarasu, and M. Saffman, An architecture for quantum networking of neutral atom processors, Appl. Phys. B **128**, 151 (2022).

[13] J. P. Covey, H. Weinfurter, and H. Bernien, Quantum networks with neutral atom processing nodes, npj Quantum Inf. **9**, 90 (2023).

[14] R. Nigmatullin, C. J. Ballance, N. De Beaudrap, and S. C. Benjamin, Minimally complex ion traps as modules for quantum communication and computing, New J. Phys. **18**, 103028 (2016).

[15] I. V. Inlek, C. Crocker, M. Lichtman, K. Sosnova, and C. Monroe, Multispecies trapped-ion node for quantum networking, Phys. Rev. Lett. **118**, 250502 (2017).

[16] A. Reiserer, N. Kalb, M. S. Blok, K. J. M. van Bemmelen, T. H. Taminiau, R. Hanson, D. J. Twitchen, and M. Markham, Robust quantum-network memory using decoherence-protected subspaces of nuclear spins, Phys. Rev. X **6**, 021040 (2016).

[17] P.-J. Stas, Y. Q. Huan, B. Machielse, E. N. Knall, A. Suleymanzade, B. Pingault, M. Sutula, S. W. Ding, C. M. Knaut, D. R. Assumpcao *et al.*, Robust multi-qubit quantum network node with integrated error detection, Science **378**, 557 (2022).

[18] G. Wendin, Quantum information processing with superconducting circuits: a review, Rep. Prog. Phys. **80**, 106001 (2017).

[19] F. Arute, K. Arya, R. Babbush, D. Bacon, J. C. Bardin, R. Barends, R. Biswas, S. Boixo, F. G. S. L. Brandao, D. A. Buell

et al., Quantum supremacy using a programmable superconducting processor, Nature (London) **574**, 505 (2019).

[20] X. Xue, M. Russ, N. Samkharadze, B. Undseth, A. Sammak, G. Scappucci, and L. M. K. Vandersypen, Quantum logic with spin qubits crossing the surface code threshold, Nature (London) **601**, 343 (2022).

[21] G. Burkard, T. D. Ladd, A. Pan, J. M. Nichol, and J. R. Petta, Semiconductor spin qubits, Rev. Mod. Phys. **95**, 025003 (2023).

[22] P. Wang, C.-Y. Luan, M. Qiao, M. Um, J. Zhang, Y. Wang, X. Yuan, M. Gu, J. Zhang, and K. Kim, Single ion qubit with estimated coherence time exceeding one hour, Nat. Commun. **12**, 233 (2021).

[23] K. R. Brown, J. Kim, and C. Monroe, Co-designing a scalable quantum computer with trapped atomic ions, npj Quantum Inf. **2**, 16034 (2016).

[24] C. D. Bruzewicz, J. Chiaverini, R. McConnell, and J. M. Sage, Trapped-ion quantum computing: Progress and challenges, Appl. Phys. Rev. **6** (2019).

[25] M. Morgado and S. Whitlock, Quantum simulation and computing with rydberg-interacting qubits, AVS Quantum Sci. **3** (2021).

[26] T. D. Ladd, F. Jelezko, R. Laflamme, Y. Nakamura, C. Monroe, and J. L. O'Brien, Quantum computers, Nature (London) **464**, 45 (2010).

[27] N. M. Linke, D. Maslov, M. Roetteler, S. Debnath, C. Figgatt, K. A. Landsman, K. Wright, and C. Monroe, Experimental comparison of two quantum computing architectures, Proc. Natl. Acad. Sci. USA **114**, 3305 (2017).

[28] Exact times vary wildly between the many different implementations of a solid-state or atom-based qubit and even within a given type of qubit. For instance, the coherence and gate times of semiconductor spin qubits (a type of solid-state qubit) vary significantly depending on the implementation, say whether the qubits used are encoded in ensembles or single-spins, nuclear or electronic spins, etc. [17,21]. Also note that in neutral atom quantum computing with Rydberg qubits, the gate and coherence times tend to be longer than for ions yet still much shorter than superconducting circuits [25]. See Ref. [27] for one specific careful comparison of quantum computations on five superconducting transmon qubits versus five trapped ion qubits. Our point here is to indicate the often present large difference in the orders of magnitude for gate and coherence times in these technologies.

[29] P. Rabl, D. DeMille, J. M. Doyle, M. D. Lukin, R. J. Schoelkopf, and P. Zoller, Hybrid quantum processors: Molecular ensembles as quantum memory for solid state circuits, Phys. Rev. Lett. **97**, 033003 (2006).

[30] M. Wallquist, K. Hammerer, P. Rabl, M. Lukin, and P. Zoller, Hybrid quantum devices and quantum engineering, Phys. Scr. **2009**, 014001 (2009).

[31] Z.-L. Xiang, S. Ashhab, J. Q. You, and F. Nori, Hybrid quantum circuits: Superconducting circuits interacting with other quantum systems, Rev. Mod. Phys. **85**, 623 (2013).

[32] G. Kurizki, P. Bertet, Y. Kubo, K. Mølmer, D. Petrosyan, P. Rabl, and J. Schmiedmayer, Quantum technologies with hybrid systems, Proc. Natl. Acad. Sci. USA **112**, 3866 (2015).

[33] N. Maring, P. Farrera, K. Kutluer, M. Mazzera, G. Heinze, and H. de Riedmatten, Photonic quantum state transfer between a cold atomic gas and a crystal, Nature (London) **551**, 485 (2017).

[34] P. Scarlino, D. J. Van Woerkom, U. C. Mendes, J. V. Koski, A. J. Landig, C. K. Andersen, S. Gasparinetti, C. Reichl, W. Wegscheider, K. Ensslin *et al.*, Coherent microwave-photon-mediated coupling between a semiconductor and a superconducting qubit, Nat. Commun. **10**, 3011 (2019).

[35] A. A. Clerk, K. W. Lehnert, P. Bertet, J. R. Petta, and Y. Nakamura, Hybrid quantum systems with circuit quantum electrodynamics, Nat. Phys. **16**, 257 (2020).

[36] N. Lauk, N. Sinclair, S. Barzanjeh, J. P. Covey, M. Saffman, M. Spiropulu, and C. Simon, Perspectives on quantum transduction, Quantum Sci. Technol. **5**, 020501 (2020).

[37] D. Awschalom, K. K. Berggren, H. Bernien, S. Bhave, L. D. Carr, P. Davids, S. E. Economou, D. Englund, A. Faraon, M. Fejer *et al.*, Development of quantum interconnects (QUICS) for next-generation information technologies, PRX Quantum **2**, 017002 (2021).

[38] A. Kumar, A. Suleymanzade, M. Stone, L. Taneja, A. Anferov, D. I. Schuster, and J. Simon, Quantum-enabled millimetre wave to optical transduction using neutral atoms, Nature (London) **615**, 614 (2023).

[39] C. Weedbrook, S. Pirandola, R. García-Patrón, N. J. Cerf, T. C. Ralph, J. H. Shapiro, and S. Lloyd, Gaussian quantum information, Rev. Mod. Phys. **84**, 621 (2012).

[40] Y. Chu and S. Gröblacher, A perspective on hybrid quantum opto-and electromechanical systems, Appl. Phys. Lett. **117**, 150503 (2020).

[41] K. Stannigel, P. Komar, S. J. M. Habraken, S. D. Bennett, M. D. Lukin, P. Zoller, and P. Rabl, Optomechanical quantum information processing with photons and phonons, Phys. Rev. Lett. **109**, 013603 (2012).

[42] A. Zivari, N. Fiaschi, R. Burgwal, E. Verhagen, R. Stockill, and S. Gröblacher, On-chip distribution of quantum information using traveling phonons, Sci. Adv. **8**, eadd2811 (2022).

[43] A. Bienfait, K. J. Satzinger, Y. P. Zhong, H.-S. Chang, M.-H. Chou, C. R. Conner, É. Dumur, J. Grebel, G. A. Peairs, R. G. Povey *et al.*, Phonon-mediated quantum state transfer and remote qubit entanglement, Science **364**, 368 (2019).

[44] M. Lucamarini, Z. L. Yuan, J. F. Dynes, and A. J. Shields, Overcoming the rate–distance limit of quantum key distribution without quantum repeaters, Nature (London) **557**, 400 (2018).

[45] M. Pittaluga, M. Minder, M. Lucamarini, M. Sanzaro, R. I. Woodward, M.-J. Li, Z. Yuan, and A. J. Shields, 600-km repeater-like quantum communications with dual-band stabilization, Nat. Photon. **15**, 530 (2021).

[46] P. Kurpiers, P. Magnard, T. Walter, B. Royer, M. Pechal, J. Heinsoo, Y. Salathé, A. Akin, S. Storz, J.-C. Besse *et al.*, Deterministic quantum state transfer and remote entanglement using microwave photons, Nature (London) **558**, 264 (2018).

[47] C. J. Axline, L. D. Burkhart, W. Pfaff, M. Zhang, K. Chou, P. Campagne-Ibarcq, P. Reinhold, L. Frunzio, S. M. Girvin, L. Jiang *et al.*, On-demand quantum state transfer and entanglement between remote microwave cavity memories, Nat. Phys. **14**, 705 (2018).

[48] P. Campagne-Ibarcq, E. Zalys-Geller, A. Narla, S. Shankar, P. Reinhold, L. Burkhart, C. Axline, W. Pfaff, L. Frunzio, R. J. Schoelkopf *et al.*, Deterministic remote entanglement

of superconducting circuits through microwave two-photon transitions, Phys. Rev. Lett. **120**, 200501 (2018).

[49] N. Leung, Y. Lu, S. Chakram, R. K. Naik, N. Earnest, R. Ma, K. Jacobs, A. N. Cleland, and D. I. Schuster, Deterministic bidirectional communication and remote entanglement generation between superconducting qubits, npj Quantum Inf. **5**, 18 (2019).

[50] H.-S. Chang, Y. P. Zhong, A. Bienfait, M.-H. Chou, C. R. Conner, É. Dumur, J. Grebel, G. A. Peairs, R. G. Povey, K. J. Satzinger *et al.*, Remote entanglement via adiabatic passage using a tunably dissipative quantum communication system, Phys. Rev. Lett. **124**, 240502 (2020).

[51] Y. Zhong, H.-S. Chang, A. Bienfait, É. Dumur, M.-H. Chou, C. R. Conner, J. Grebel, R. G. Povey, H. Yan, D. I. Schuster *et al.*, Deterministic multi-qubit entanglement in a quantum network, Nature (London) **590**, 571 (2021).

[52] L. D. Burkhart, J. D. Teoh, Y. Zhang, C. J. Axline, L. Frunzio, M. H. Devoret, L. Jiang, S. M. Girvin, and R. J. Schoelkopf, Error-detected state transfer and entanglement in a superconducting quantum network, PRX Quantum **2**, 030321 (2021).

[53] M. Casariego, E. Z. Cruzeiro, S. Gherardini, T. Gonzalez-Raya, R. André, G. Frazão, G. Catto, M. Möttönen, D. Datta, K. Viisanen *et al.*, Propagating quantum microwaves: towards applications in communication and sensing, Quantum Sci. Technol. **8**, 023001 (2023).

[54] G. Vallone, D. Bacco, D. Dequal, S. Gaiarin, V. Luceri, G. Bianco, and P. Villoresi, Experimental satellite quantum communications, Phys. Rev. Lett. **115**, 040502 (2015).

[55] J. Yin, Y. Cao, Y.-H. Li, S.-K. Liao, L. Zhang, J.-G. Ren, W.-Q. Cai, W.-Y. Liu, B. Li, H. Dai *et al.*, Satellite-based entanglement distribution over 1200 kilometers, Science **356**, 1140 (2017).

[56] Y.-A. Chen, Q. Zhang, T.-Y. Chen, W.-Q. Cai, S.-K. Liao, J. Zhang, K. Chen, J. Yin, J.-G. Ren, Z. Chen *et al.*, An integrated space-to-ground quantum communication network over 4,600 kilometres, Nature (London) **589**, 214 (2021).

[57] L. de Forges de Parny, O. Alibart, J. Debaud, S. Gressani, A. Lagarrigue, A. Martin, A. Metrat, M. Schiavon, T. Troisi, E. Diamanti *et al.*, Satellite-based quantum information networks: use cases, architecture, and roadmap, Commun. Phys. **6**, 12 (2023).

[58] T. Gonzalez-Raya, M. Casariego, F. Fesquet, M. Renger, V. Salari, M. Möttönen, Y. Omar, F. Deppe, K. G. Fedorov, and M. Sanz, Open-air microwave entanglement distribution for quantum teleportation, Phys. Rev. Appl. **18**, 044002 (2022).

[59] A. G. Radnaev, Y. O. Dudin, R. Zhao, H. H. Jen, S. D. Jenkins, A. Kuzmich, and T. A. B. Kennedy, A quantum memory with telecom-wavelength conversion, Nat. Phys. **6**, 894 (2010).

[60] K. Heshami, D. G. England, P. C. Humphreys, P. J. Bustard, V. M. Acosta, J. Nunn, and B. J. Sussman, Quantum memories: emerging applications and recent advances, J. Mod. Opt. **63**, 2005 (2016).

[61] A. Wallucks, I. Marinković, B. Hensen, R. Stockill, and S. Gröblacher, A quantum memory at telecom wavelengths, Nat. Phys. **16**, 772 (2020).

[62] E. Arenskötter, T. Bauer, S. Kucera, M. Bock, J. Eschner, and C. Becher, Telecom quantum photonic interface for a $^{40}Ca^{+}$ single-ion quantum memory, npj Quantum Inf. **9**, 34 (2023).

[63] H.-J. Briegel, W. Dür, J. I. Cirac, and P. Zoller, Quantum repeaters: The role of imperfect local operations in quantum communication, Phys. Rev. Lett. **81**, 5932 (1998).

[64] L.-M. Duan, M. D. Lukin, J. I. Cirac, and P. Zoller, Long-distance quantum communication with atomic ensembles and linear optics, Nature (London) **414**, 413 (2001).

[65] W. J. Munro, K. Azuma, K. Tamaki, and K. Nemoto, Inside quantum repeaters, IEEE J. Sel. Top. Quantum Electron. **21**, 78 (2015).

[66] In contrast to wave packet shaping methods, quantum state transfer by adiabatic passage between two cavities via an intermediate fiber (channel), which is also deterministic, can mitigate losses due to absorption in the cavities [79,141,142]. However, consideration of the hybridization of such an adiabatic passage based QST scheme for a case where transduction is needed is beyond the scope of this work.

[67] K. Randles and S. J. van Enk, Quantum state transfer and input-output theory with time reversal, Phys. Rev. A **108**, 012421 (2023).

[68] See Supplemental Material at http://link.aps.org/supplemental/10.1103/PhysRevA.110.012415 for further discussion of the scope of our results, the possible wave packets that are producible, and how known error correction schemes can be incorporated, which includes Refs. [1,33,37,43,46–48,51–53,59,60,62,67,70,73–75,77,80,81,84,85,87,89,92–94,94,97,98,98–105,122–124,140,143–186].

[69] Note that more general wave packet shaping may be necessary in some scenarios [94,123,143] (say for interfacing with fibers), though in our case, and to realize many hybrid quantum interfaces, the time reversal and stretching operations are sufficient.

[70] J. I. Cirac, P. Zoller, H. J. Kimble, and H. Mabuchi, Quantum state transfer and entanglement distribution among distant nodes in a quantum network, Phys. Rev. Lett. **78**, 3221 (1997).

[71] C. Monroe, D. M. Meekhof, B. E. King, W. M. Itano, and D. J. Wineland, Demonstration of a fundamental quantum logic gate, Phys. Rev. Lett. **75**, 4714 (1995).

[72] D. J. Wineland, C. Monroe, W. M. Itano, D. Leibfried, B. E. King, and D. M. Meekhof, Experimental issues in coherent quantum-state manipulation of trapped atomic ions, J. Res. Natl. Inst. Stand. Technol. **103**, 259 (1998).

[73] H. J. Kimble, Strong interactions of single atoms and photons in cavity QED, Phys. Scr. **1998**, 127 (1998).

[74] S. J. Van Enk, J. I. Cirac, and P. Zoller, Ideal quantum communication over noisy channels: A quantum optical implementation, Phys. Rev. Lett. **78**, 4293 (1997).

[75] S. J. Van Enk, J. I. Cirac, and P. Zoller, Photonic channels for quantum communication, Science **279**, 205 (1998).

[76] C. W. Gardiner and M. J. Collett, Input and output in damped quantum systems: Quantum stochastic differential equations and the master equation, Phys. Rev. A **31**, 3761 (1985).

[77] C. W. Gardiner, A. S. Parkins, and P. Zoller, Wave-function quantum stochastic differential equations and quantum-jump simulation methods, Phys. Rev. A **46**, 4363 (1992).

[78] C. Gardiner and P. Zoller, *Quantum Noise: A Handbook of Markovian and Non-Markovian Quantum Stochastic Methods with Applications to Quantum Optics* (Springer, Berlin, 2004).

[79] B. Vogell, B. Vermersch, T. E. Northup, B. P. Lanyon, and C. A. Muschik, Deterministic quantum state transfer between remote qubits in cavities, Quantum Sci. Technol. **2**, 045003 (2017).

[80] V. Krutyanskiy, M. Galli, V. Krcmarsky, S. Baier, D. A. Fioretto, Y. Pu, A. Mazloom, P. Sekatski, M. Canteri, M. Teller *et al.*, Entanglement of trapped-ion qubits separated by 230 meters, Phys. Rev. Lett. **130**, 050803 (2023).

[81] V. Krutyanskiy, M. Canteri, M. Meraner, J. Bate, V. Krcmarsky, J. Schupp, N. Sangouard, and B. P. Lanyon, Telecom-wavelength quantum repeater node based on a trapped-ion processor, Phys. Rev. Lett. **130**, 213601 (2023).

[82] P. C. Humphreys, N. Kalb, J. P. J. Morits, R. N. Schouten, R. F. L. Vermeulen, D. J. Twitchen, M. Markham, and R. Hanson, Deterministic delivery of remote entanglement on a quantum network, Nature (London) **558**, 268 (2018).

[83] R. Stockill, M. J. Stanley, L. Huthmacher, E. Clarke, M. Hugues, A. J. Miller, C. Matthiesen, C. L. Gall, and M. Atatüre, Phase-tuned entangled state generation between distant spin qubits, Phys. Rev. Lett. **119**, 010503 (2017).

[84] T. E. Northup and R. Blatt, Quantum information transfer using photons, Nat. Photon. **8**, 356 (2014).

[85] A. Reiserer and G. Rempe, Cavity-based quantum networks with single atoms and optical photons, Rev. Mod. Phys. **87**, 1379 (2015).

[86] E. Brion, L. H. Pedersen, and K. Mølmer, Adiabatic elimination in a lambda system, J. Phys. A: Math. Theor. **40**, 1033 (2007).

[87] This unidirectionality can be imposed using a circulator as proposed by Refs. [70,145] and used by some microwave implementations [46–48] or by directing signal reflected by system 2 down a different spatial mode, say using a ring cavity geometry. Even if we do not explicitly impose unidirectionality, the presence of a $a_2 a_1^\dagger$ term does not necessarily doom the QST scheme [51]. This is because, just as the present term has the implicit time dependence $a_2^\dagger(t)a_1(t-\tau)$ (with τ the time delay for light propagating between the nodes), the opposing term behaves as $a_2(t)a_1^\dagger(t+\tau)$. Thus, even if reflection from node 2 occurs, we would not be driving the corresponding transition for node 1 to reabsorb the now transformed photon wave packet. [Note this is only true for wave packets that are short relative to τ, as is often the case optically. Additional considerations may be warranted, e.g., Ref. [106]'s use of a circulator helps them ensure the photon is emitted into a Markovian environment (channel).] Accordingly, quantum state transfer and remote entanglement generation experiments often do not use circulators in practice, especially as they come with their own losses and errors, e.g., those due to back reflections.

[88] Here we take the position of the unitary transformation device to be coincident with system 1. Yet this can readily be generalized to any position along the transmission line between the two systems without affecting our ultimate effective description. Additionally, we have already eliminated the temporal delay between the systems (τ in Ref. [87]) by working with corresponding time-delayed variables and operators [67].

[89] M. G. Raymer, D. V. Reddy, S. J. van Enk, and C. J. McKinstrie, Time reversal of arbitrary photonic temporal modes via nonlinear optical frequency conversion, New J. Phys. **20**, 053027 (2018).

[90] A. S. Parkins, P. Marte, P. Zoller, and H. J. Kimble, Synthesis of arbitrary quantum states via adiabatic transfer of zeeman coherence, Phys. Rev. Lett. **71**, 3095 (1993).

[91] This is the wave packet in a rotating frame for the cavity modes at their respective laser frequencies [67]. The corresponding wave packet in the Schrödinger picture is $\Psi_S(t) = e^{-i\omega_{L1}t}\Psi(t)$ such that during the transformation, assuming the transformation parameters are ideal, $\Psi_S(t_s < t < t_f) = \sqrt{\gamma_2}e^{-i\omega_{L2}t}\beta_1(\xi(T-t))e^{i\zeta T}$, which makes the shift in central frequency from ω_{L1} to ω_{L2}, decay rate change from γ_1 to γ_2, and time reversal manifest (up to the known phase $e^{i\zeta T}$).

[92] G. F. Peñas, R. Puebla, and J. J. García-Ripoll, Improving quantum state transfer: correcting non-markovian and distortion effects, Quantum Sci. Technol. **8**, 045026 (2023).

[93] A. V. Gorshkov, A. André, M. D. Lukin, and A. S. Sørensen, Photon storage in Λ-type optically dense atomic media. I. Cavity model, Phys. Rev. A **76**, 033804 (2007).

[94] O. Morin, M. Körber, S. Langenfeld, and G. Rempe, Deterministic shaping and reshaping of single-photon temporal wave functions, Phys. Rev. Lett. **123**, 133602 (2019).

[95] The probability of photon loss due to the unitary transformation itself, e.g., due to absorption or scattering at U or if U is intrinsically probabilistic, is implicitly accounted for by the potential subnormalization of the wave packet incident on node 2, Ψ. For a given setup this can be made more explicit if an underlying transformation device efficiency $0 \leqslant \eta_U \leqslant 1$ can be characterized, then one can simply map $P_3 \to \eta_U P_3$.

[96] These values come from optical and telecom attenuation rates in the ranges of $0.17 \leqslant X_{\text{tele}} \leqslant 0.3$ dB/km and $3 \leqslant X_{\text{opt}} \leqslant 3.5$ dB/km [62,79,81], respectively, which are translated to our notation via $x_{\text{tl}}^{-1} = X\ln(10)/10$.

[97] H. Takahashi, E. Kassa, C. Christoforou, and M. Keller, Strong coupling of a single ion to an optical cavity, Phys. Rev. Lett. **124**, 013602 (2020).

[98] S. Ritter, C. Nölleke, C. Hahn, A. Reiserer, A. Neuzner, M. Uphoff, M. Mücke, E. Figueroa, J. Bochmann, and G. Rempe, An elementary quantum network of single atoms in optical cavities, Nature (London) **484**, 195 (2012).

[99] A. Reiserer, S. Ritter, and G. Rempe, Nondestructive detection of an optical photon, Science **342**, 1349 (2013).

[100] A. Reiserer, N. Kalb, G. Rempe, and S. Ritter, A quantum gate between a flying optical photon and a single trapped atom, Nature (London) **508**, 237 (2014).

[101] H. Chibani, Photon blockade with memory and slow light using a single atom in an optical cavity, Ph.D. thesis, Technische Universität München, 2016.

[102] S. Daiss, S. Langenfeld, S. Welte, E. Distante, P. Thomas, L. Hartung, O. Morin, and G. Rempe, A quantum-logic gate between distant quantum-network modules, Science **371**, 614 (2021).

[103] M. Steiner, H. M. Meyer, J. Reichel, and M. Köhl, Photon emission and absorption of a single ion coupled to an optical-fiber cavity, Phys. Rev. Lett. **113**, 263003 (2014).

[104] S. Begley, M. Vogt, G. K. Gulati, H. Takahashi, and M. Keller, Optimized multi-ion cavity coupling, Phys. Rev. Lett. **116**, 223001 (2016).

[105] X. Han, W. Fu, C.-L. Zou, L. Jiang, and H. X. Tang, Microwave-optical quantum frequency conversion, Optica **8**, 1050 (2021).

[106] P. Magnard, S. Storz, P. Kurpiers, J. Schär, F. Marxer, J. Lütolf, T. Walter, J.-C. Besse, M. Gabureac, K. Reuer *et al.*, Microwave quantum link between superconducting circuits housed in spatially separated cryogenic systems, Phys. Rev. Lett. **125**, 260502 (2020).

[107] For more general interfaces between systems with different Hamiltonians and hence different system controls, we cannot simply use Eq. (16). Rather we must engineer a new laser pulse (or other relevant system controls), which we can do by *again* leveraging the fact that absorption is the time reversed process to emission. That is, just as we can tailor the system controls for node 1 (G_1 here) to produce a certain wave packet [$\Psi(t) = \sqrt{\gamma_1}\beta_1(t)$ here; see SM Sec. B3], we can likewise, in a time-reversed analogous fashion, tailor the system 2 controls (G_2 here) so that node 2 absorbs an incoming wave packet. Depending on the specific systems and intermediate wave packet, this may be probabilistic at best.

[108] We choose to define the complex conjugated Green's function, $\Gamma^*(t,t')$, so that Eq. (23) takes a more standard form for a complex inner product.

[109] This whole argument applies more generally as long as the EOM for the analog of α_2 is linear and there is an ideal solution with $|\alpha_2^i(t_e)| = 1$.

[110] S. Biswas and S. J. van Enk, Detecting two photons with one molecule, Phys. Rev. A **104**, 043703 (2021).

[111] H. Ball, W. D. Oliver, and M. J. Biercuk, The role of master clock stability in quantum information processing, npj Quantum Inf. **2**, 16033 (2016).

[112] R. Valivarthi, M. li Grimau Puigibert, Q. Zhou, G. H. Aguilar, V. B. Verma, F. Marsili, M. D. Shaw, S. W. Nam, D. Oblak, and W. Tittel, Quantum teleportation across a metropolitan fibre network, Nat. Photon. **10**, 676 (2016).

[113] J. S. Lundeen, A. Feito, H. Coldenstrodt-Ronge, K. L. Pregnell, Ch. Silberhorn, T. C. Ralph, J. Eisert, M. B. Plenio, and I. A. Walmsley, Tomography of quantum detectors, Nat. Phys. **5**, 27 (2009).

[114] H. B. Coldenstrodt-Ronge, J. S. Lundeen, K. L. Pregnell, A. Feito, B. J. Smith, W. Mauerer, C. Silberhorn, J. Eisert, M. B. Plenio, and I. A. Walmsley, A proposed testbed for detector tomography, J. Mod. Opt. **56**, 432 (2009).

[115] C. M. Natarajan, L. Zhang, H. Coldenstrodt-Ronge, G. Donati, S. N. Dorenbos, V. Zwiller, I. A. Walmsley, and R. H. Hadfield, Quantum detector tomography of a time-multiplexed superconducting nanowire single-photon detector at telecom wavelengths, Opt. Express **21**, 893 (2013).

[116] S. J. van Enk, Photodetector figures of merit in terms of povms, J. Phys. Commun. **1**, 045001 (2017).

[117] S. M. Young, M. Sarovar, and F. Léonard, General modeling framework for quantum photodetectors, Phys. Rev. A **98**, 063835 (2018).

[118] T. B. Propp and S. J. van Enk, Quantum networks for single photon detection, Phys. Rev. A **100**, 033836 (2019).

[119] K. Kraus, A. Böhm, J. D. Dollard, and W. H. Wootters, *States, Effects, and Operations Fundamental Notions of Quantum Theory: Lectures in Mathematical Physics at the University of Texas at Austin* (Springer, Berlin, 1983).

[120] K. Jacobs and D. A. Steck, A straightforward introduction to continuous quantum measurement, Contemp. Phys. **47**, 279 (2006).

[121] M. A. Nielsen and I. L. Chuang, *Quantum Computation and Quantum Information* (Cambridge University Press, Cambridge, 2010).

[122] J. Lavoie, J. M. Donohue, L. G. Wright, A. Fedrizzi, and K. J. Resch, Spectral compression of single photons, Nat. Photon. **7**, 363 (2013).

[123] R. W. Andrews, A. P. Reed, K. Cicak, J. D. Teufel, and K. W. Lehnert, Quantum-enabled temporal and spectral mode conversion of microwave signals, Nat. Commun. **6**, 10021 (2015).

[124] M. Allgaier, V. Ansari, L. Sansoni, C. Eigner, V. Quiring, R. Ricken, G. Harder, B. Brecht, and C. Silberhorn, Highly efficient frequency conversion with bandwidth compression of quantum light, Nat. Commun. **8**, 14288 (2017).

[125] S.-C. Chan and J.-M. Liu, Tunable narrow-linewidth photonic microwave generation using semiconductor laser dynamics, IEEE J. Sel. Top. Quantum Electron. **10**, 1025 (2004).

[126] S. W. Brown, G. P. Eppeldauer, and K. R. Lykke, Facility for spectral irradiance and radiance responsivity calibrations using uniform sources, Appl. Opt. **45**, 8218 (2006).

[127] M. A. Tran, D. Huang, J. Guo, T. Komljenovic, P. A. Morton, and J. E. Bowers, Ring-resonator based widely-tunable narrow-linewidth Si/InP integrated lasers, IEEE J. Sel. Top. Quantum Electron. **26**, 1500514 (2019).

[128] M. Corato-Zanarella, A. Gil-Molina, X. Ji, M. C. Shin, A. Mohanty, and M. Lipson, Widely tunable and narrow-linewidth chip-scale lasers from near-ultraviolet to near-infrared wavelengths, Nat. Photon. **17**, 157 (2023).

[129] W. Chen, J. Cousin, E. Poullet, J. Burie, D. Boucher, X. Gao, M. W. Sigrist, and F. K. Tittel, Continuous-wave mid-infrared laser sources based on difference frequency generation, C. R. Phys. **8**, 1129 (2007).

[130] M. A. Belkin, F. Capasso, A. Belyanin, D. L. Sivco, A. Y. Cho, D. C. Oakley, C. J. Vineis, and G. W. Turner, Terahertz quantum-cascade-laser source based on intracavity difference-frequency generation, Nat. Photon. **1**, 288 (2007).

[131] Reference [187] uses and analyzes this index in a much different, neuroscience-based context, though such a measure is often considered in principal component analysis, in which case this index is the percent of variance captured by the first principal component of the data. Such an index is quite natural based on the Eckart-Young theorem [188] for low-rank matrix approximations [189]. An analogous quantity often considered in quantum information, e.g., in multipartite entanglement characterization, is the "Schmidt number," which is encoded in the Schmidt decomposition (which is nothing but a singular value decomposition in disguise) of a quantum state [190]. See SM Sec. C for further method details and discussion.

[132] This is analogous to Eq. (3) of Ref. [74] using our notation for the states (they consider emitters with a slightly modified level structure compared to the Λ-type systems we consider due to the presence of an additional ground state). Note that Υ_2 errors can be mapped onto Υ_1 errors by performing the local operation $|e_1\rangle \to |g_1\rangle$ after the transmission, say via optically pumping, then we obtain a map of the same form as Eq. (3) of Ref. [75].

[133] M. H. Michael, M. Silveri, R. T. Brierley, V. V. Albert, J. Salmilehto, L. Jiang, and S. M. Girvin, New class of quantum

error-correcting codes for a bosonic mode, Phys. Rev. X **6**, 031006 (2016).
[134] N. H. Lindner and T. Rudolph, Proposal for pulsed on-demand sources of photonic cluster state strings, Phys. Rev. Lett. **103**, 113602 (2009).
[135] Y. Zhan and S. Sun, Deterministic generation of loss-tolerant photonic cluster states with a single quantum emitter, Phys. Rev. Lett. **125**, 223601 (2020).
[136] P. Thomas, L. Ruscio, O. Morin, and G. Rempe, Efficient generation of entangled multiphoton graph states from a single atom, Nature (London) **608**, 677 (2022).
[137] J. Preskill, Quantum computing in the NISQ era and beyond, Quantum **2**, 79 (2018).
[138] A. N. Craddock, J. Hannegan, D. P. Ornelas-Huerta, J. D. Siverns, A. J. Hachtel, E. A. Goldschmidt, J. V. Porto, Q. Quraishi, and S. L. Rolston, Quantum interference between photons from an atomic ensemble and a remote atomic ion, Phys. Rev. Lett. **123**, 213601 (2019).
[139] A. M. Dyckovsky and S. Olmschenk, Analysis of photon-mediated entanglement between distinguishable matter qubits, Phys. Rev. A **85**, 052322 (2012).
[140] M. Pompili, S. L. N. Hermans, S. Baier, H. K. C. Beukers, P. C. Humphreys, R. N. Schouten, R. F. L. Vermeulen, M. J. Tiggelman, L. dos Santos Martins, B. Dirkse *et al.*, Realization of a multinode quantum network of remote solid-state qubits, Science **372**, 259 (2021).
[141] T. Pellizzari, Quantum networking with optical fibres, Phys. Rev. Lett. **79**, 5242 (1997).
[142] S. J. Van Enk, H. J. Kimble, J. I. Cirac, and P. Zoller, Quantum communication with dark photons, Phys. Rev. A **59**, 2659 (1999).
[143] D. Kielpinski, J. F. Corney, and H. M. Wiseman, Quantum optical waveform conversion, Phys. Rev. Lett. **106**, 130501 (2011).
[144] T. B. Propp and S. J. van Enk, How to project onto an arbitrary single-photon wave packet, Phys. Rev. A **102**, 053707 (2020).
[145] C. W. Gardiner, Driving a quantum system with the output field from another driven quantum system, Phys. Rev. Lett. **70**, 2269 (1993).
[146] H. J. Carmichael, Quantum trajectory theory for cascaded open systems, Phys. Rev. Lett. **70**, 2273 (1993).
[147] J. Dalibard, Y. Castin, and K. Mølmer, Wave-function approach to dissipative processes in quantum optics, Phys. Rev. Lett. **68**, 580 (1992).
[148] K. Mølmer, Y. Castin, and J. Dalibard, Monte Carlo wave-function method in quantum optics, J. Opt. Soc. Am. B **10**, 524 (1993).
[149] M. Pechal, L. Huthmacher, C. Eichler, S. Zeytinoğlu, A. A. Abdumalikov, Jr., S. Berger, A. Wallraff, and S. Filipp, Microwave-controlled generation of shaped single photons in circuit quantum electrodynamics, Phys. Rev. X **4**, 041010 (2014).
[150] E. T. Jaynes and F. W. Cummings, Comparison of quantum and semiclassical radiation theories with application to the beam maser, Proc. IEEE **51**, 89 (1963).
[151] D. Meschede, H. Walther, and G. Müller, One-atom maser, Phys. Rev. Lett. **54**, 551 (1985).
[152] A. Reiserer, Colloquium: Cavity-enhanced quantum network nodes, Rev. Mod. Phys. **94**, 041003 (2022).
[153] A. D. Boozer, A. Boca, R. Miller, T. E. Northup, and H. J. Kimble, Reversible state transfer between light and a single trapped atom, Phys. Rev. Lett. **98**, 193601 (2007).
[154] S. Welte, B. Hacker, S. Daiss, S. Ritter, and G. Rempe, Photon-mediated quantum gate between two neutral atoms in an optical cavity, Phys. Rev. X **8**, 011018 (2018).
[155] P. Samutpraphoot, T. Đorđević, P. L. Ocola, H. Bernien, C. Senko, V. Vuletić, and M. D. Lukin, Strong coupling of two individually controlled atoms via a nanophotonic cavity, Phys. Rev. Lett. **124**, 063602 (2020).
[156] A. Stute, B. Casabone, B. Brandstätter, K. Friebe, T. E. Northup, and R. Blatt, Quantum-state transfer from an ion to a photon, Nat. Photon. **7**, 219 (2013).
[157] L. J. Stephenson, D. P. Nadlinger, B. C. Nichol, S. An, P. Drmota, T. G. Ballance, K. Thirumalai, J. F. Goodwin, D. M. Lucas, and C. J. Ballance, High-rate, high-fidelity entanglement of qubits across an elementary quantum network, Phys. Rev. Lett. **124**, 110501 (2020).
[158] J. Schupp, V. Krcmarsky, V. Krutyanskiy, M. Meraner, T. E. Northup, and B. P. Lanyon, Interface between trapped-ion qubits and traveling photons with close-to-optimal efficiency, PRX Quantum **2**, 020331 (2021).
[159] K. Hammerer, A. S. Sørensen, and E. S. Polzik, Quantum interface between light and atomic ensembles, Rev. Mod. Phys. **82**, 1041 (2010).
[160] T. Neuman, M. Eichenfield, M. E. Trusheim, L. Hackett, P. Narang, and D. Englund, A phononic interface between a superconducting quantum processor and quantum networked spin memories, npj Quantum Inf. **7**, 121 (2021).
[161] J. Larson and Th. K. Mavrogordatos, *The Jaynes-Cummings Model and its Descendants: Modern Research Directions* (IoP Publishing, Bristol, 2021).
[162] K. Reuer, J.-C. Besse, L. Wernli, P. Magnard, P. Kurpiers, G. J. Norris, A. Wallraff, and C. Eichler, Realization of a universal quantum gate set for itinerant microwave photons, Phys. Rev. X **12**, 011008 (2022).
[163] M. Khanbekyan and D.-G. Welsch, Cavity-assisted spontaneous emission of a single Λ-type emitter as a source of single-photon packets with controlled shape, Phys. Rev. A **95**, 013803 (2017).
[164] K. A. G. Fisher, D. G. England, J.-P. W. MacLean, P. J. Bustard, K. J. Resch, and B. J. Sussman, Frequency and bandwidth conversion of single photons in a room-temperature diamond quantum memory, Nat. Commun. **7**, 11200 (2016).
[165] R. A. Maruf, S. Venuturumilli, D. Bharadwaj, P. Anderson, J. Qiu, Y. Yuan, M. Zeeshan, B. Semnani, P. J. Poole, D. Dalacu *et al.*, Widely tunable solid-state source of single-photons matching an atomic transition, arXiv:2309.06734.
[166] W. Huie, S. G. Menon, H. Bernien, and J. P. Covey, Multiplexed telecommunication-band quantum networking with atom arrays in optical cavities, Phys. Rev. Res. **3**, 043154 (2021).
[167] V. Krutyanskiy, M. Meraner, J. Schupp, and B. P. Lanyon, Polarisation-preserving photon frequency conversion from a trapped-ion-compatible wavelength to the telecom C-band, Appl. Phys. B **123**, 228 (2017).
[168] R. Ikuta, T. Kobayashi, T. Kawakami, S. Miki, M. Yabuno, T. Yamashita, H. Terai, M. Koashi, T. Mukai, T. Yamamoto

et al., Polarization insensitive frequency conversion for an atom-photon entanglement distribution via a telecom network, Nat. Commun. **9**, 1997 (2018).

[169] M. Bock, P. Eich, S. Kucera, M. Kreis, A. Lenhard, C. Becher, and J. Eschner, High-fidelity entanglement between a trapped ion and a telecom photon via quantum frequency conversion, Nat. Commun. **9**, 1998 (2018).

[170] F. Kaiser, P. Vergyris, A. Martin, D. Aktas, M. P. De Micheli, O. Alibart, and S. Tanzilli, Quantum optical frequency up-conversion for polarisation entangled qubits: towards interconnected quantum information devices, Opt. Express **27**, 25603 (2019).

[171] P. Forn-Diaz, C. W. Warren, C. W. S. Chang, A. M. Vadiraj, and C. M. Wilson, On-demand microwave generator of shaped single photons, Phys. Rev. Appl. **8**, 054015 (2017).

[172] R. W. Andrews, R. W. Peterson, T. P. Purdy, K. Cicak, R. W. Simmonds, C. A. Regal, and K. W. Lehnert, Bidirectional and efficient conversion between microwave and optical light, Nat. Phys. **10**, 321 (2014).

[173] R. Sahu, W. Hease, A. Rueda, G. Arnold, L. Qiu, and J. M. Fink, Quantum-enabled operation of a microwave-optical interface, Nat. Commun. **13**, 1276 (2022).

[174] M. Mirhosseini, A. Sipahigil, M. Kalaee, and O. Painter, Superconducting qubit to optical photon transduction, Nature (London) **588**, 599 (2020).

[175] R. D. Delaney, M. D. Urmey, S. Mittal, B. M. Brubaker, J. M. Kindem, P. S. Burns, C. A. Regal, and K. W. Lehnert, Superconducting-qubit readout via low-backaction electro-optic transduction, Nature (London) **606**, 489 (2022).

[176] A. Kyle, C. L. Rau, W. D. Warfield, A. Kwiatkowski, J. D. Teufel, K. W. Lehnert, and T. Dennis, Optically distributing remote two-node microwave entanglement using doubly parametric quantum transducers, Phys. Rev. Appl. **20**, 014005 (2023).

[177] B. B. Blinov, D. L. Moehring, L.-M. Duan, and C. Monroe, Observation of entanglement between a single trapped atom and a single photon, Nature (London) **428**, 153 (2004).

[178] B. Brecht, D. V. Reddy, C. Silberhorn, and M. G. Raymer, Photon temporal modes: A complete framework for quantum information science, Phys. Rev. X **5**, 041017 (2015).

[179] H. P. Specht, J. Bochmann, M. Mücke, B. Weber, E. Figueroa, D. L. Moehring, and G. Rempe, Phase shaping of single-photon wave packets, Nat. Photon. **3**, 469 (2009).

[180] P. Müller, T. Tentrup, M. Bienert, G. Morigi, and J. Eschner, Spectral properties of single photons from quantum emitters, Phys. Rev. A **96**, 023861 (2017).

[181] C. Ferreira and J. L. López, Asymptotic expansions of the Hurwitz–Lerch zeta function, J. Math. Anal. Appl. **298**, 210 (2004).

[182] C. H. Bennett, G. Brassard, C. Crépeau, R. Jozsa, A. Peres, and W. K. Wootters, Teleporting an unknown quantum state via dual classical and Einstein-Podolsky-Rosen channels, Phys. Rev. Lett. **70**, 1895 (1993).

[183] C. H. Bennett, G. Brassard, S. Popescu, B. Schumacher, J. A. Smolin, and W. K. Wootters, Purification of noisy entanglement and faithful teleportation via noisy channels, Phys. Rev. Lett. **76**, 722 (1996).

[184] C. Hamsen, K. N. Tolazzi, T. Wilk, and G. Rempe, Two-photon blockade in an atom-driven cavity QED system, Phys. Rev. Lett. **118**, 133604 (2017).

[185] E. Deist, Y.-H. Lu, J. Ho, M. K. Pasha, J. Zeiher, Z. Yan, and D. M. Stamper-Kurn, Mid-circuit cavity measurement in a neutral atom array, Phys. Rev. Lett. **129**, 203602 (2022).

[186] M. Keller, B. Lange, K. Hayasaka, W. Lange, and H. Walther, Continuous generation of single photons with controlled waveform in an ion-trap cavity system, Nature (London) **431**, 1075 (2004).

[187] D. A. Depireux, J. Z. Simon, D. J. Klein, and S. A. Shamma, Spectro-temporal response field characterization with dynamic ripples in ferret primary auditory cortex, J. Neurophysiol. **85**, 1220 (2001).

[188] C. Eckart and G. Young, The approximation of one matrix by another of lower rank, Psychometrika **1**, 211 (1936).

[189] G. Strang, *Linear Algebra and Learning from Data* (SIAM, Philadelphia, 2019).

[190] K. Zielnicki, K. Garay-Palmett, D. Cruz-Delgado, H. Cruz-Ramirez, M. F. O'Boyle, B. Fang, V. O. Lorenz, A. B. U'Ren, and P. G. Kwiat, Joint spectral characterization of photon-pair sources, J. Mod. Opt. **65**, 1141 (2018).